



UNIVERSIDAD DE INVESTIGACIÓN DE TECNOLOGÍA EXPERIMENTAL YACHAY

Escuela de Ciencias Químicas e Ingeniería

Synthesis and Characterization of Chitosan Aerogels for Removal of Cr(VI) from Wastewater

Trabajo de integración curricular presentado como requisito para la
obtención del título de Ingeniero en Polímeros

Autor/a:

Danny Steven Peñaloza Tinoco

Tutor/a:

MSc. Lola De Lima

Cotutor/a:

PhD. Floralba López

Urcuquí, junio del 2023

Autoría

Yo, **Danny Peñaloza**, con cédula de identidad 0705336527, declaro que las ideas, juicios, valoraciones, interpretaciones, consultas bibliográficas, definiciones y conceptualizaciones expuestas en el presente trabajo; así como los procedimientos y herramientas utilizadas en la investigación son de absoluta responsabilidad de el autor del trabajo de integración curricular. Así mismo, me acojo a los reglamentos internos de la Universidad de Investigación de Tecnología Experimental Yachay.

Urcuquí, mayo del 2023.

Danny Steven Peñaloza Tinoco

CI: 0705336527

Autorización de publicación

Yo, **Danny Peñaloza**, con cédula de identidad 0705336527, cedo a la Universidad de Investigación de Tecnología Experimental Yachay, los derechos de publicación de la presente obra, sin que deba haber un reconocimiento económico por este concepto. Declaro además que el texto del presente trabajo de titulación no podrá ser cedido a ninguna empresa editorial para su publicación u otros fines, sin contar previamente con la autorización escrita de la Universidad.

Asimismo, autorizo a la Universidad que realice la digitalización y publicación de este trabajo de integración curricular en el repositorio virtual, de conformidad a lo dispuesto en el Art. 144 de la Ley Orgánica de Educación

Urcuquí, mayo del 2023.

Danny Steven Peñaloza Tinoco

CI: 0705336527

Dedication

I would like to dedicate this work to all those people who supported and accompanied me on my university journey, especially my dear family. To my parents, because without their moral and financial support, I would not have been able to achieve this goal. To my grandmother, Lastenia, aunt, Mariuxi, and uncle, Jasmany, since they always watched over me, and since I was little, they boosted and motivated me to fulfill my aspirations.

To my angels, Maruja and Celena, for taking care of me and being proud of me until their last minutes here on Earth. To my siblings, for making my days happier and I hope it will inspire them to complete their personal aspirations.

To my friends and future colleagues for making this journey full of memorable and funny moments, especially Maria I. Cruz, Daniela de Llano, Milene Gonzalez, and Karen Alban I will always carry you in my heart; to my roommates Carlos, José, Daniel, Rubén, and Sebastian for being supportive friends and accompany me during the days of study and entertainment.

Danny Steven Peñaloza Tinoco

Acknowledgment

I would like to thank to my parents and professors for all their support to accomplished this step in my life. My parents help and effort let me achieve this new stage in life and served as an inspiration to always finished every single goal that i have. I am also very greatfull with my advisors Ph.D. Rose Mary Michell and M.Sc. Lola de Lima and my co-advisor Ph.D. Floralba Lopez for their guidance during the process of constructing this project; all their support was invaluable and help me to developed this research work. I have acquired a lot of experience and knowledge of every suggestion and correction they made. I also want to express my gratitude to every professor that i have during my career, for their support, enthusiasm and patient in teaching me about science, professional life and ethic. Finally, I am very grateful with my family for their unconditional support especially to my grandmother, Lastenia, for being by my side in every step of my life and always in care of me.

Danny Steven Peñaloza Tinoco

Resumen

En este trabajo se presenta un método de síntesis sol-gel para obtener un aerogel a base de quitosano preparado con ácido cítrico como agente de entrecruzamiento, y probando varias ratios entre las materias primas durante el proceso. Los aerogeles sintetizados se caracterizaron por FTIR, TGA y SEM para analizar su estructura, composición y morfología. Para evaluar la capacidad de adsorción del material se realizaron pruebas de hinchazón y adsorción. Los estudios con FTIR y TGA han demostrado que el quitosano se entrecruzó con éxito en un rango particular de proporción quitosano:ácido cítrico (Ch:Ca) entre 2:1 y 5:1, observándose un aumento en el entrecruzamiento con el incremento de ácido cítrico. Durante los ensayos de adsorción de Cr(VI), la adsorción óptima la consiguió el aerogel con la relación Ch:Ca de 5:1 (Ch5Ca1). El estudio cinético determinó que el mecanismo de adsorción tiene un mejor ajuste al Pseudo-Segundo-Orden (PSO), por lo que el mecanismo sugerido es la adsorción química, con un tiempo de adsorción óptimo de 110 minutos. Por otro lado, el modelo de isotérmico se ajusta mejor al modelo de Redlich-Peterson, indicando que la homogeneidad energética de los aerogeles preparados se va degradando a medida que aumenta la temperatura. Esto se asume por la tendencia decreciente del factor β de Redlich-Peterson a medida que aumenta la temperatura. Finalmente, todas las propiedades termodinámicas determinadas fueron menores a cero, para el cambio de energía libre de Gibbs (ΔG°) indica la espontaneidad del proceso de adsorción, y para el cambio de entalpía (ΔH°) sugiere que el proceso es exotérmico. Sin embargo, el valor negativo para el cambio de entropía (ΔS°) sugiere que durante el proceso de adsorción los grados de libertad del sistema disminuyen y, por lo tanto, el sistema se ordena.

Palabras Clave:

Aerogeles, quitosano, ácido cítrico, adsorción de cromo (VI), tratamiento de agua

Abstract

In this work is presented a sol-gel synthesis method to obtain a chitosan-based aerogel prepared with citric acid as the crosslinking agent, testing various ratios of raw materials during the process. The synthesized aerogels were characterized by FTIR, TGA, and SEM to analyze their structure, composition, and morphology while swelling and adsorption tests were carried out to evaluate the adsorption capacity of the material. FTIR and TGA studies have shown that the chitosan was successfully cross-linked in a particular range of chitosan-citric acid (Ch:Ca) ratios between 2:1 to 5:1, observing an increase in crosslinking with the increasing proportion of citric acid. During the Cr(VI) adsorption tests, the optimal adsorption was achieved by the aerogel with the proportion Ch:Ca of 5:1 codified as Ch5Ca1. Kinetics evaluations determined that the adsorption mechanism fits better with the Pseudo-Second-Order (PSO), so the mechanism suggested is chemical adsorption, with an optimal adsorption time of 110 minutes. On the other hand, the adsorption isotherm model with the best fit corresponds to the Redlich-Peterson model, indicating that the energy homogeneity of aerogels prepared degrades as the temperature increase. This is assumed by the decreasing trend of the Redlich-Peterson β factor as the temperature is increased. Finally, all determined thermodynamic properties were below zero, which for the Gibbs free energy change (ΔG°) indicates the spontaneity of the adsorption process, and for the enthalpy change (ΔH°) suggests that the process is exothermic. However, the negative value for the entropy change (ΔS°) suggests that during the adsorption process, the system's degrees of freedom decrease, and therefore the system orders.

Keywords:

Aerogels, chitosan, citric acid, chromium (VI) adsorption, water treatment

Contents

Dedication	iii
Acknowledgment	iv
Resumen	v
Abstract	vi
Contents	vii
List of Tables	x
List of Figures	xi
List of Symbols	xv
1 Introduction	1
1.1 Problem Statement	3
1.2 Objectives	4
1.2.1 General Objective	4
1.2.2 Specific Objectives	4
2 Theoretical Background	5
2.1 Heavy Metals	5
2.1.1 Chromium contamination	6
2.2 Aerogels	9
2.2.1 Chitosan: properties, advantages, and applications	10
2.2.2 Citric acid as chitosan cross-linking agent	13

2.3	Adsorption process	14
2.3.1	Adsorption models	14
2.3.2	Adsorption kinetics	17
2.3.3	Adsorption thermodynamics	19
3	Methodology	20
3.1	Materials and Reagents	20
3.2	Aerogels Synthesis	20
3.3	Aerogels characterization	21
3.3.1	Fourier transform infrared spectroscopy (FTIR)	21
3.3.2	Thermogravimetric analysis (TGA)	22
3.3.3	Cr(VI) adsorption analysis	22
3.3.4	Scanning Electron Microscopy (SEM)	22
3.4	Swelling Of Chitosan Aerogels	23
3.5	Adsorption evaluation	23
3.5.1	Calibration curve	23
3.5.2	Adsorption kinetic	24
3.5.3	Adsorption isotherms	25
4	Results and Discussion	27
4.1	Synthesis analysis	27
4.2	Crosslinking analysis	29
4.2.1	Fourier transform infrared spectroscopy (FTIR) analysis	29
4.2.2	Thermogravimetric analysis (TGA)	30
4.3	Swelling capacity analysis	32
4.4	Chitosan aerogel selection	34
4.5	Morphological analysis	36
4.5.1	Scanning Electron Microscopy (SEM) analysis	36
4.6	Adsorption analysis	37
4.6.1	Factors affecting Cr(VI) adsorption	37
4.6.2	Cr(VI) adsorption kinetic study	41
4.6.3	Cr(VI) adsorption equilibrium study	43

4.6.4	Cr(VI) adsorption thermodynamic study	47
4.7	Economic study	49
5	Conclusions	51
	Bibliography	53

List of Tables

2.1	Eight common heavy metals and their related anthropological activities. [29]	6
2.2	Uses of the stables forms of chromium. [10]	7
3.1	Nomenclature of the different synthesized aerogels and their weighted raw materials.	21
4.1	Kinetic adsorption parameters and root-mean-square error (RMSE) for Cr(VI) removal from the PFO and PSO models.	43
4.2	Adsorption isotherm fitting parameters found from Langmuir, Freundlich, and Redlich-Peterson models at different temperatures for Cr(VI) adsorption by Ch5Ca1 aerogel.	47
4.3	Thermodynamic equilibrium constants and parameters for Cr(VI) adsorption into Ch5Ca1 samples obtained by Langmuir equation method.	48
4.4	Raw materials for the synthesis of the aerogels with their annual demand and price.	50

List of Figures

2.1	Illustration for the common preparation of aerogels. [56]	11
2.2	Illustration of the chemical structure of chitosan.	12
2.3	Illustration of the a) chemical and b) physical crosslinking mechanism on chitosan by citric acid. [65]	14
3.1	Block diagram representation of the methodology followed for the study.	26
4.1	Image of the 2% chitosan solution.	27
4.2	Image of the 2% chitosan solution.	28
4.3	Images of the hydrogel consistency achieved after the cooling process.	28
4.4	Image of the lyophilization process.	29
4.5	Comparison of FITR graphs of the synthesized chitosan aerogels in the range of 4000 to 400 cm^{-1} .	30
4.6	Comparison of FITR graphs between the synthesized chitosan aerogels and citric acid powder in the range of 1800 to 1600 cm^{-1} .	31
4.7	Comparison of Thermogravimetric analysis (TGA) plots of the synthesized chitosan aerogels.	32
4.8	Comparison of Derivate thermogravimetric (DTA) plots of the synthesized chitosan aerogels.	33
4.9	Swelling kinetic plots of the Ch5Ca1, Ch3Ca1 & Ch2Ca1 synthesized chitosan aerogels.	34
4.10	Illustration of a chitosan aerogel before and after the Cr(VI) adsorption process.	35
4.11	Comparison of Cr(VI) adsorption of the Ch5Ca1, Ch3Ca1, and Ch2Ca1 synthesized aerogels in 5 mg/L chromium solutions.	35

4.12	Scanning electron microscope images of Ch5Ca1 aerogel at 250x and 2000x	36
4.13	Effect of the initial concentration on the Cr(VI) adsorption capacity of the Ch5Ca1 aerogel, for a loading ratio of 20 mg/50 mL at 20 °C.	38
4.14	Effect of adsorbent weight : adsorbate solution volume ratio (loading ratio) on the adsorption of 50 mL of Cr(VI) solution by Ch5Ca1 aerogel.	39
4.15	Effect of adsorbent weight : adsorbate solution volume ratio (loading ratio) on the adsorption capacity (q_e) of 50 mL of Cr(VI) solution by Ch5Ca1 aerogel. Experimental data plotted at 1 ppm (squares) and 10 ppm (circles) Cr(VI) concentrations.	40
4.16	Effect of temperature on the Cr(VI) adsorption capacity of the Ch5Ca1 aerogel.	41
4.17	PFO (a) and PSO (b) fitted models to data obtained for the adsorption of 10 ppm Cr(VI) with a loading ratio of 20 mg/ 50 mL at 20 °C. Experimental data plotted by both non-linear (squares) and linear (circles) representation model.	42
4.18	Langmuir adsorption isotherm plots for Cr(VI) adsorption by Ch5Ca1 sample at temperatures: 20 (a), 30 (b), 37 °C (c). Experimental data plotted by both non-linear (squares) and linear (circles) representation model. . . .	44
4.19	Freundlich adsorption isotherm plots for Cr(VI) adsorption by Ch5Ca1 sample at temperatures: 20 (a), 30 (b), 37 °C (c). Experimental data plotted by both non-linear (squares) and linear (circles) representation model. . . .	45
4.20	Redlich-Peterson adsorption isotherm plots for Cr(VI) adsorption by Ch5Ca1 sample at temperatures: 20 (a), 30 (b), 37 °C (c). Experimental data plotted by both non-linear (squares) and linear (circles) representation model. . . .	46
4.21	Block diagram process for the chitosan aerogel synthesis.	49

List of Symbols

α	Rendlich-Peterson's constant
β	Rendlich-Peterson's exponent constant
ΔG°	Gibbs free energy change
ΔH°	Enthalpy change
ΔS°	Entropy change
ϵ	Adsorption coefficient
Θ	Fraction of the surface covered at equilibrium
A	Absorbance
AAS	Atomic Absorption Spectroscopy
ATR	Attenuated total reflectance
C	Concentration
C_e	Equilibrium concentration
C_i	Initial concentration
C_t	Final concentration
Ca	Citric acid
Ch	Chitosan
C°	Standard state concentration

DTG	Differential thermogravimetric analysis
E_{sr}	Water absorption percentage
FTIR	Fourier Transform Infrared Spectroscopy
INEN	Instituto Nacional Ecuatoriano de Normalizaci3n
k_1	Equilibrium rate constant in the PFO
k_2	Equilibrium rate constant in the PSO
K_F	Freundlich's adsorption constant
K_{HE}	Henry's adsorption constant
K_L	Langmuir's adsorption constant
K_{RP}	Rendlich-Peterson's adsorption constant
K°	Standard equilibrium constant
l	Optical path length
n	Freundlich's adsorption intensity
PFO	Pseudo-First-Order
PSO	Pseudo-Second-Order
q_e	Adsorption capacity at equilibrium
q_m	Maximum adsorption capacity
q_t	Adsorption capacity at time t
R	Universal gas constant
SEM	Scanning Electron Microscopy
t	time
TGA	Termogravimetric analysis

UV-Vis UV-Vis Adsorption Spectroscopy

V Volume

W Sample weight

W_d Sample's dry weight

W_s Sample's swollen weight

WHO World Health Organization

Chapter 1

Introduction

Water, known as the fundamental liquid for life, is currently used for any of the industrial processes or domestic activities [1]. Nevertheless, water is of great concern due to the amount of pollutants that are being released in the principal water bodies (rivers, lakes, oceans), caused by domestic, agricultural, and industrial activities [2]. Industries like textile dyeing, pharmaceutical industries, leather tanning, fertilizer industries, and mining industries, among others generated wastewater in a big amount of around 400 billion m^3/year [3]. These wastes contain a lot of toxic contaminants such as heavy metals, dyes, salts, nitrogen, and phosphorous content contributing to the high level of toxicity.[1, 4] Therefore, it seriously affects the use of water sources and the aquatic environment of the ecosystem [5], and in prolonged contact with humans or animals, pollutants can lead to several infections, carcinogenic effects, itching, breathing problems, vision loss, etc [4]. Thus, due to its complexity, efficient technology for industrial waste management is crucial.

Particularly, heavy metals play a significant role as pollutants due to their ability to remain in the environment for long periods of time [2]; even in the food chain, the bio-accumulation of heavy metals is a common phenomenon, since they are non-biodegradables [6]. Rivers contamination by heavy metals is alarming in many countries, and Ecuador is not an exception, most rivers present high levels of arsenic, chromium, plumber, cadmium, mercury, copper, and zinc [7, 8, 9]. In this thesis, chromium was selected for the removal studies, especially chromium (VI), which is the toxic ionic form. Also, studies in Ecuador's water effluents determined that the principal activity for contamination with chromium (VI) is

tanning [10]. This activity is carried out by local companies in the central area of Ecuador, employing traditional techniques but at the same time highly contaminating processes due to chromium (VI) salts [11]. The released chromium exposure (oral, dermal, and inhalation) can lead to disastrous consequences which can result in cancer commonly or even death by poisoning [12, 13].

Therefore, heavy metals removal from wastewater is essential for preserving animals and population health. In this trend, new technologies have been developing to ensure methods for heavy metal concentration control in water-treatment processes, like chemical precipitation, flotation, adsorption, coagulation-flocculation, ion-exchange, membrane filtration, and electrochemical procedures [14]. Among them adsorption method is the best option, due to its simplicity, low cost, and efficiency [15]. Although the most common adsorption material is activated carbon, all of these properties fit completely with polysaccharide-based aerogels, which additionally present high adsorption capacities for metal ions pollutants because of their functional groups [16]. One of the most common polysaccharides is chitin, which is the second most abundant in the world, typically extracted from exoskeletons of arthropods [17]. After a desacetylation process, chitin is transformed into chitosan [18]. Chitosan has properties such as low cost of manufacture, renewable, non-toxicity, biodegradability, hydrophilicity, high reactivity coagulation, flocculation, and biosorption capabilities (through its amino and hydroxide groups) that make it an eco-friendly adsorbent [19].

Since 2011 chitosan-based aerogels are the second most researched aerogel polysaccharide, and even the studies for environmental engineering applications cover more than 30% overall [16]. China is the leading country in publications focusing on the application of aerogels for wastewater treatment. Most of the studies focus on modifications to enhance the adsorption capacities [20, 21] or the use of a second material to achieve a synergism effect, such as graphene or graphene oxide [22], cellulose (any-form) [23] and bentonite [24], among others.

In this thesis project, is proposed a simple and cheap synthesis method of chitosan aerogel

by a citric acid cross-linking agent through the sol-gel method. Furthermore, the adsorption capacity was evaluated by varying parameters such as temperature and solute concentration. Additionally, the material characterization was made via Fourier transform infrared spectrometry (FTIR), Thermogravimetric analysis (TGA) to confirm cross-linking, Scanning Electron Microscopy (SEM) for the morphology analysis, and swelling tests for the swollen degree determination. Finally, kinetic, equilibrium (isotherm), and thermodynamic studies were developed to understand the behavior of the chitosan aerogels at chromium (VI) solutions.

1.1 Problem Statement

As is known, water is fundamental for living beings. Today human activities are releasing huge amounts of chemicals, and typically poisoning the principal water effluents (rivers, lakes, oceans). All these pollutants can be in contact with humans, fauna, and flora causing affections on their health.

Some of the major pollutants are heavy metals, such as lead (Pb), arsenic (As), mercury (Hg), chromium (Cr) especially hexavalent chromium (Cr (VI)), nickel (Ni), barium (Ba), cadmium (Cd), cobalt (Co), selenium (Se), vanadium (V), which just in small quantities are very toxic [25]. Additionally, they can remain in the environment and tend to bio-accumulate, making them difficult to remove.

In Ecuador, the principal heavy metal contamination activities are mining, textile, and leather industries. This last one releases huge quantities of chromium (VI) through its wastewater because of the tanning process [11]. This process is carried out in a traditional and unsanitary way, using highly toxic chromium salts. Chromium (VI) contact, any kind (oral, dermal & inhalation) can lead to hazardous consequences, degrading human health and typically causing cancer [26].

Limitations on the chromium content are obligatory to regulate the contamination. According to the World Health Organization water bodies have the limit of 0.05 mg/L chromium

(VI) concentration [27], and Ecuador follows this measure. To deal with the problematic water-treatment processes must be employed to reduce the pollution concentration, for heavy metals the use of adsorbents is the best and most common option. Furthermore, the nowadays environmentally friendly tendency can be covered through the use of bio-adsorbents.

Consequently, this thesis project focused on developing a cheap bio-adsorbent and evaluating its adsorption capacity at chromium (VI) solutions.

1.2 Objectives

1.2.1 General Objective

Synthesis and characterization of chitosan-based aerogels for chromium (IV) removal from aqueous solution.

1.2.2 Specific Objectives

- To develop a sol-gel process for the synthesis of aerogels of chitosan with citric acid as a cross-linking agent.
- To analyze the behavior of aerogels of chitosan and citric acid at different ratios.
- To determine the optimal chitosan-citric acid ratio for the adsorption of Cr (VI).
- To evaluate the kinetics, isothermal equilibrium, and thermodynamic behavior during the chromium (VI) adsorption.
- To understand the adsorption mechanism of the adsorbent.

Chapter 2

Theoretical Background

2.1 Heavy Metals

Metals can be essential for the health and survival of all living beings but are of a lot of concern because many of them have toxic properties [28]. Metals are intrinsic components of the environment [29]. These factors and a wide toxicological evaluation for metals, taking into account basic concepts of toxicity and variability in sensitivity to deficiency, determine intervals of (low) daily intake and limited intake. Based on this, metals can be classified as essential, beneficial, or detrimental. Some essential metals for human health are iron, zinc, copper, chromium, iodine, cobalt, molybdenum, and selenium, but in trace proportions [28]. An inadequate supply can lead to a variety of deficiency diseases or syndromes [30].

Heavy metals refers to a block of all the metals in Group 3 to 16 that are in periods 4 or higher, they may also be known as the transition and post-transition metals [31]. Some authors relate them to metals having an atomic weight greater than 40.04 (the atomic mass of Ca) [32] or to electronegative metals with a density higher than 5 g/cm³ [29]. Opposite to common metals, heavy metals are very harmful and toxic even at ppb (parts per billion) range [25]. Table 2.1 exposed the principal human activities related to heavy metals contamination to the environment.

Heavy metals enter the environment by natural and anthropic means, these last such as

Table 2.1: Eight common heavy metals and their related anthropological activities. [29]

Source	As	Cd	Cr	Cu	Pb	Hg	Ni	Zn
Mining and ore processing	+	+	-	+	-	+	-	+
Metallurgy	+	+	+	+	+	+	+	+
Chemical industry	+	+	+	+	+	+	-	+
Alloys industry	-	-	-	-	+	-	-	-
Paint industry	-	+	+	-	+	-	-	+
Glass industry	+	-	-	-	+	+	-	-
Pulp and paper industry	-	-	+	+	+	+	+	-
Leather tanning	+	-	+	-	-	+	-	+
Textile dyeing and printing	+	+	-	+	+	+	+	+
Fertilizer industry	+	+	+	+	+	+	+	+
Chloro-alkali industry	+	+	+	-	+	+	-	+
Petroleum refining	+	+	+	+	+	+	-	+
Coal burning	+	+	+	+	+	+	+	-

+ : related activity; - : non-related activity

mining, industrial discharge, urban runoff, pest or disease control agents, and air contamination fallout, among others [32]. Contamination can also be produced by metal corrosion, atmospheric deposition, soil erosion of metal ions and leaching of heavy metals, sediment re-suspension and metal evaporation from water resources to soil and groundwater [33]. The industrial contamination sources include metal processing refineries, activities related to petroleum extraction, nuclear power stations, plastics, textiles, electronics circuits, wood preservation, and paper industries [30]. By all this contamination, since the last century has been studying processes for the remediation of the polluted soil [34] and water effluents [29]. An innovative and environmentally friendly method is bioabsorption or the use of bioadsorbents [35, 36]. Other methods for the removal of heavy metals are inverse osmosis, metal reduction, or the use of adsorbents [37].

2.1.1 Chromium contamination

Chromium is known as the most abundant mineral in Earth's crust, being found in almost all oxidation states ranging from -2 to +6 [38], but only the elemental (0), the trivalent and hexavalent forms are the most stable, although the divalent form is common with air contact is easily oxidized to the trivalent form [39]. But only, chromium (III) and (VI) are important in the effects on human health. Biological affections by elemental chromium

cannot be made. [39] Table 2.2 resumes the typical uses of chromium in its three stable forms, and it can be determined that the general main uses for chromium are metallurgical (67%), refractories (18%), and chemical (15%) [10].

Table 2.2: Uses of the stables forms of chromium. [10]

Form	Uses
Chromium (0)	Metal and alloy manufacturing, stainless steel production, alloy production
Chromium (III)	Metal and alloy manufacturing, chrome plating, leather tanning, textiles, brick lining, copy machine toner
Chromium (VI)	Chrome plating, leather tanning, textiles, copy machine toner

Natural chromium hardly ever produces a hazard to human health, because it is found in soil and plants and as a part of animal feed as chromium (III), being part of the human diet. Human affections by chromium mostly occur due to Cr(VI) chemical compound exposure, so it is the principal cause of a toxic response [39, 40]. While information about the use of chromium (III) in the industrial process targets its derivative compounds as irritants [39].

Before the XXI century, a lot of research was made to determine the mechanism of the allergenic, carcinogenic, and irritant effects of chromium. For example, chromium (III) was observed to play an important role in many biological processes, and its human oral intake resulted in a 99% recovery in the feces [41]. While for the Cr(VI) intake, in the form of sodium chromate, the fecal recovery was only 90%, indicating a 10% of the dose is absorbed by the gastrointestinal tract [41]. Therefore, a limited oral intake must be considered in order to keep in good health, the dosage was established at 33-45 $\mu\text{g}/\text{day}$ for infants (< 1 year), 123-171 $\mu\text{g}/\text{day}$ for children (< 10 years) and 246-343 $\mu\text{g}/\text{day}$ for adults [42]. Another way of chromium exposure is by air, according to the study of Aitio et al. (1988) [43] there is a correlation between the Cr(VI) and urinary excretion in workers of the chrome plating industry, even the rate uptake is directly related to the solubility of the chromium (VI) source. Furthermore, topical application of chromium salts (in the study case sodium sulfate) can also create retention of Cr(VI) [26]. Further studies on chromium

(VI) found that it is not produced in nature and all the contamination is produced by human activities [38]. To sum up, chromium (VI) contamination can be found in air, soil, and water.

Water contamination is the critical exposure route, because compared to the other ones it can easily be distributed to the entire population through oral exposure [40]. Additionally, oral chromium (VI) exposure can be classified into three types through its duration, these are acute (14 days or less), intermediate (75 - 365 days), and chronic (365 days or more), while the health effects can be categorized in carcinogenic and non-carcinogenic [12].

In Ecuador, chromium (VI) contamination is mainly due to the leather industry, during the tanning process. Tanning is a process of transforming raw animal skins into leather by using chromium sulfate, which may be one of human's oldest technologies [10][40], and currently is used in almost 90% of all tanned leather produced worldwide [40]. The exaggerated dosage of the chemical products involve in tanning, the bad practices of manufacturing, and the poor personal training are the factors that generate high contamination of the residual waters [11].

Additionally, studies in Ecuador effluents revealed a high concentration of chromium (VI), which was used for the population, agriculture, and livestock [37, 44]. Their values exceeded the Ecuadorian regulations, which according to the "Instituto Nacional Ecuatoriano de Normalización 1108" (INEN 1108) is established at 0.05 mg/L [45], this value is the same that for the World Health Organization (WHO) [27]. According to Portilla. A. (2013) [11], who studied the tanning process at a small company in Ambato, determined that using the traditional tanning process, the company produces 2 to 5 kg of chromium per ton of rawhide, while an advanced proposed process, only produces 0.05 to 0.1 kg of chromium per ton of rawhide. Although, water contamination by the tanning process is the main source of Cr(VI), the contamination by dyes, paints, organic and agro-industry waste, plastic, glass, and scrap metal, among others are polluting the dump's soil with chromium (trivalent and hexavalent) [46].

Materials with high sorption capacity are of main interest in the area of heavy metal capture, particularly the ones cheap, affordable, and easy to synthesize. The principal employed material is activated carbon, but currently, aerogels are being studied since has higher adsorption capacity [47].

2.2 Aerogels

Aerogels are a light material made from a tridimensional structure through a freeze-dried process, their raw materials can be inorganic or organic [48]. The first time an aerogel was synthesized was in 1931 by S.S. Kistler, who succeeded in designing gels in which the liquid was removed by applying a supercritical drying process [49]. Then, this method was improved in order to produce aerogels from water-glass by Teichner's group, during the process they employed tetramethoxysilane-alcohol-water mixture as a starting solution [50]. There have been 92 years of a lot of research in the area, and new trends and applications have been studied in the process. Some of the nowadays research applications of aerogels are thermal insulation, sound insulation, capacitor electrode, carrier for various materials catalysts, solar cells, and adsorbents for removal of organic and inorganic pollutants from wastewater [51].

Nowadays, according to Smirnova and Gurikov (2018) [52] aerogels are defined as polymeric or open colloidal networks which are formed of bonded and loosely particles or fibers that expanded themselves by air/gas and consequently have a very low density. Furthermore, aerogels are considered the lightest solid material produced at an industrial scale, having a density from 0.003 to 0.15 kg/m³ depending on the raw materials and methods involved [48, 53]. Other important aerogels properties are their high porosity and large surface areas, which are around 100 to 1600 m² [53, 54]. Conventional aerogels can be classified based on their composition, drying technologies, and advances in synthesis, dividing them into three groups: inorganic (for example SiO₂), organic (for example polyurethane), or carbon (for example graphene) [48]. Additionally, aerogels using materials from different groups are called hybrids and are synthesized in order to obtain unique properties.

Currently, sustainable aerogel materials are of main interest. The most prevalent class of organic substances on Earth are biopolymers, which are a subset of polymers made by living organisms. The distinctive three-dimensional structures of aerogels combined with the inherent benefits of biopolymers have created enticing new potential applications [55]. On the other hand, commercial aerogels are mostly produced using silica for a variety of applications [52].

The method of aerogel synthesis is called sol-gel and involved three steps which are the sol-gel reaction, aging, and drying process. Figure 2.1 resumes the steps for the biopolymer aerogels synthesis, it is appreciable that during the sol-gel reaction is important to establish the precursors and their concentrations. For the aging step temperature and time are the modifiable variables, especially temperature can play an important role in the structure formation [47, 56].

For the last step, there are three options: ambient drying, freeze-drying, and supercritical drying; and each process has its advantages and disadvantages. For ambient drying, a chemical hydrophobization of the gel structure is needed and maintains a slightly elevated temperature, having a low cost but the matrix is compacted during the process. For freeze-drying, vacuum, low temperatures (-70 to -20 °C), and the addition of a modifier are needed (avoid compaction), having a high cost, and even if the density is smaller the pore structure is partially destroyed. And finally, supercritical drying used solvents or CO₂-solvent mix, and need extreme conditions of temperature ($T > 100$ °C) or pressure ($P > 74$ bar), the process has a significant cost, is often not compatible with the aerogel and can release toxicity gases [52]. Currently, polysaccharides-based aerogels are being studied due to their excellent adsorption properties and easy preparation method [55].

2.2.1 Chitosan: properties, advantages, and applications

Polysaccharides are biopolymers of monosaccharides which are unique raw materials and have excellent properties (biocompatibility, abundant resources, low environmental loads, and flexibility for functionalization) [55]. They come in a wide range of structures and

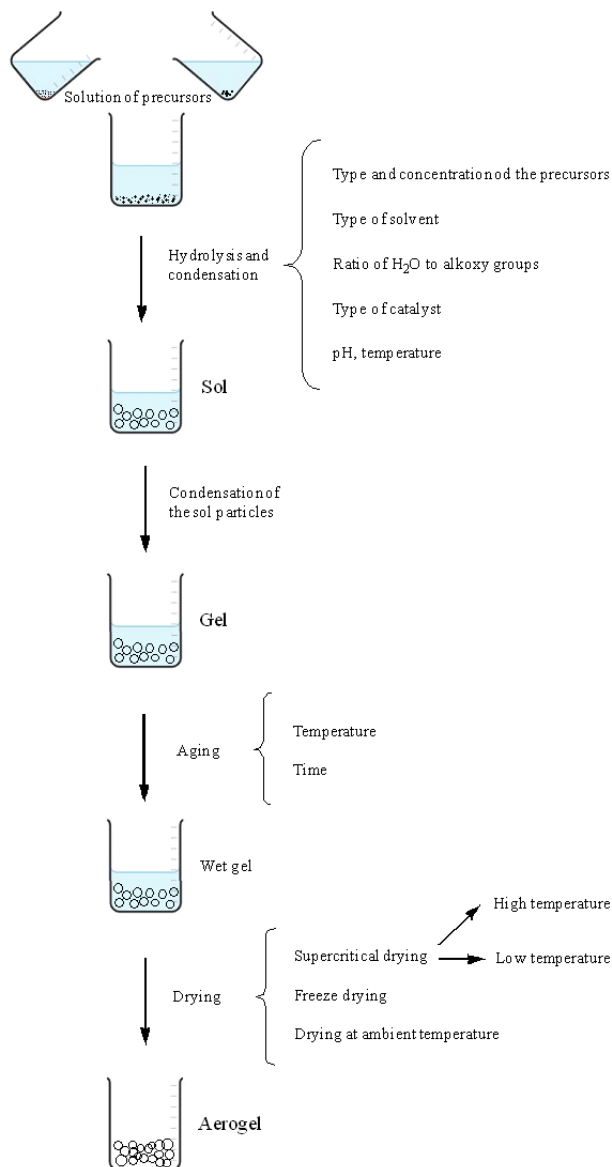


Figure 2.1: Illustration for the common preparation of aerogels. [56]

forms, and mostly are used as structural materials, these characteristics are quite different to the synthetic polymers [17]. Additionally, they possess chemical and biological qualities as non-toxicity, biocompatibility, biodegradability, polyfunctionality, high chemical reactivity, chirality, chelation, and adsorption capabilities [55]. Among all the polysaccharides, chitin and cellulose are found in larger production, which is estimated to be nearly 100 billions tons each per year, and also are the most abundant organic compounds on earth [17].

Chitin, which is commonly obtained from the exoskeletons of arthropods (crabs, lobsters and shrimps) and from the flexible internal backbone of cephalopods (internal shells of squids), is deacetylated to produce chitosan, whose structure is based on D-glucosamine connected to N-acetyl Dglucosamine by a -1,4-glycosidic bond [17, 57]. The procedure to make chitosan from chitin sources involves the following four steps: deacetylation, de-proteinization, demineralization, and decoloration [18]. The result is a biopolymer with a linear structure of 2-amino-2-deoxy-D-glucopyranose that is (1-4)-linked [58]. Chitosan has been identified as a copolymer of glucosamine and N-acetyl glucosamine as a consequence of N-deacetylation, and it is visualized in Figure 2.2 [18]. Although, chitin and chitosan exhibit excellent properties, they have limitations in their reactivity and processability [59].

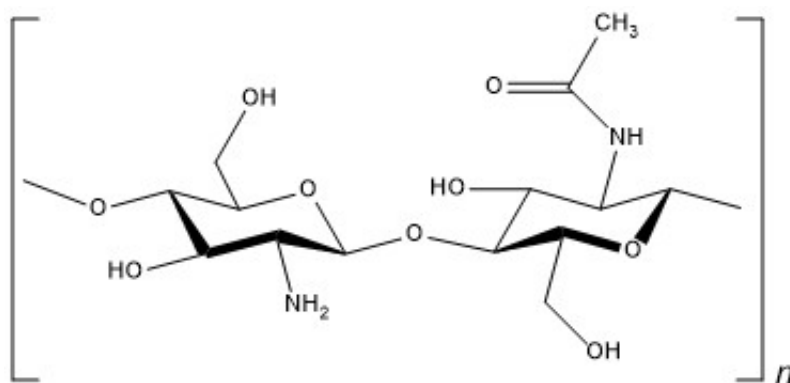


Figure 2.2: Illustration of the chemical structure of chitosan.

Numerous industries, including medicine, agriculture, cosmetics, textile, food manufacturing, biotechnology, and environmental engineering, have made extensive use of chitosan [60]. This final one has been explored for chitosan's unique static attraction and adsorption of metal ions (remarking heavy metals) and poisonous dyes that can be present in wastewater effluents, especially in the field of water treatment. Due to its amino and hydroxyl groups of chitosan, which, depending on the kind of metal ion, create chelates between metal ions and chitosan [61]. Currently, new technologies using chitosan-based material for the benefit of humans as well as the environment have been applied. In advanced applications including wound dressing, medication delivery, bone restoration, biosensors, food packaging, and water treatment, among others, aerogel has been developed from chitosan-based biopolymers [48].

2.2.2 Citric acid as chitosan cross-linking agent

Chitosan aerogels can be crosslinked using both chemical and physical networking techniques. The physical bond used in the physical networking approach is reversible and based on hydrogen bonds, ionic interactions, and molecular entanglements. Tripolyphosphate, sodium citrate, and sulfosuccinate acid are a few examples of anionic cross-linkers that are frequently utilized in this context [62]. On the other hand, chemical cross-linking can achieve micro- and nano-structures enhancing the mechanical, thermal, and chemical stability [63]. Nowadays, toxic chemical as formaldehyde, isocyanate, epoxy, and so on are used as chemical cross-linkers [64]. In certain cases, it is preferable to utilize fewer or non-toxic chemicals to cross-link biopolymers like chitosan [65].

In order to develop nontoxic materials, other crosslinking agents like sodium trimetaphosphate, sodium tripolyphosphate, phosphorus oxychloride, or carboxylic acids, have thus lately been suggested. Citric acid, which is a carboxylic acid, presents properties of nontoxicity, widespread usage as a safe natural ingredient in the food sector, and strong chemical reactivity, being an excellent material for large-scale production [55].

A variety of methods can be applied to obtain chitosan materials cross-linked with chitosan, such as casting [66], compression molding [67], emulsification [68], and sol-gel methods [56]. But the crosslinking mechanism is the same. The interaction between chitosan and citric acid is peculiar, it can have two behaviors a physical and a chemical cross-linking, even being able to compete with each other. According to Guerrero et al. (2019) [67] at elevated temperatures and dry ambient, chemical cross-linking is favored. Figure 2.3 illustrates both mechanisms, in the case of covalent cross-linking it occurs by conversion of primary amine to amide upon heat treatment of the chitosan with citric acid. While ionic cross-linking is the electrostatic interaction between a protonated amine and a carboxylate ion, expected at non-heat treatment [66].

Once the material is selected, its sorption process must be studied, evaluating behaviors such as kinetic, isotherm, and thermodynamic properties. These studies are able to mod-

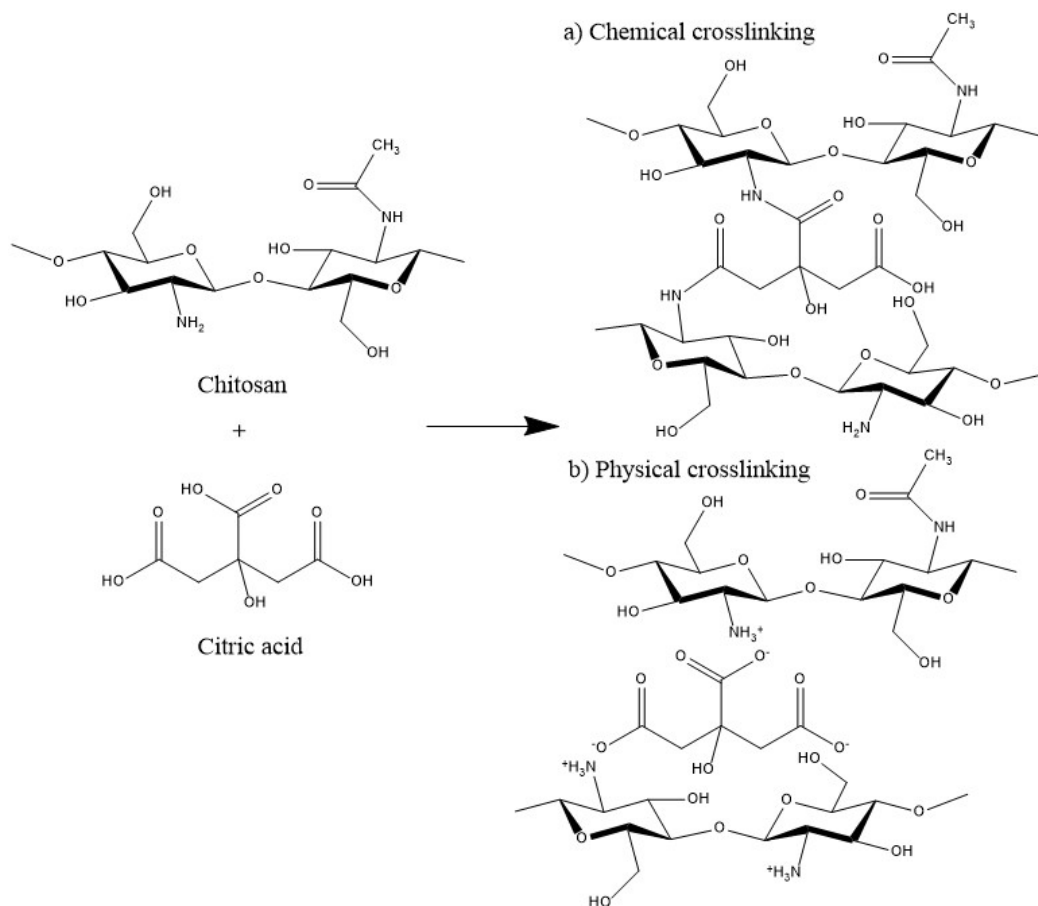


Figure 2.3: Illustration of the a) chemical and b) physical crosslinking mechanism on chitosan by citric acid. [65]

ulate and understand the mechanism and capacities of the material.

2.3 Adsorption process

Adsorption is a phenomenon that occurs on the surface of a material and it is defined as the increase in the concentration of a particular compound at the surface in a two phases interaction, commonly a solid phase with a liquid or gas phase [69].

2.3.1 Adsorption models

The study of the mechanism of adsorption is fundamental for the analysis of an adsorbent. To understand the interaction and forecast the equilibrium between the liquid (adsorbate) and solid (adsorbent) phases at a specific temperature, mathematical distributions (mod-

els) can be explored [70] The adsorption equilibrium study is the most important part of the information for a well understanding of an adsorption process. The proper interpretation of adsorption isotherms is crucial for the improvement of the adsorption system and the effective design of the adsorption process. Adsorption isotherms are represented as the number of adsorbate particles (it can be mass or moles) per amount of adsorbent (in mass units) as a function of the equilibrium concentration of the adsorbate in solution, at a constant temperature [71].

This representation of the coverage fraction of the adsorbent is carried out in order to analyze the interactions between adsorbate and adsorbent, and select an isotherm adsorption model based on theoretical premises [72]. The common models for equilibrium analysis are Temkin, Langmuir, Freundlich, and Rendlich-Peterson, in particular for chitosan adsorbents. For each case, the isotherms or equations show valuable data for fitting the modeling.

Henry model

The simplest isotherm distribution and the only one-parameter model, in which the active sites are directly proportional to the equilibrium concentration [73]. This model fits well at relatively low adsorbate concentrations, supposing that all adsorbate molecules are isolated from one another [69]. Equation 2.1 is the linear relation between the equilibrium adsorbate concentrations in both phases [72].

$$q_e = K_{HE}C_e \quad (2.1)$$

where q_e is the amount of the adsorbate at equilibrium (mg/g), K_{HE} is Henry's adsorption constant, and C_e is the equilibrium concentration of the adsorbate on the adsorbent.

Langmuir model

In 1916, Irving Langmuir created its own isotherm model, basically from empirical assumptions that the adsorbate behaves as an ideal gas, so adsorption can occur only at localized finite sites [74]. Furthermore, the surface coverage is in a monolayer structure

with a constant balancing of the relative rates of adsorption and desorption [75]. The Langmuir general equation (2.2) is as follows:

$$q_e = \frac{K_L q_m C_e}{1 + K_L C_e} \quad (2.2)$$

where K_L is the Langmuir constant related to the adsorption capacity (mg g^{-1}) and q_m is the maximum adsorption capacity of the adsorbent. Langmuir constant can be related to the area and porosity of the adsorbent material. Additionally, Langmuir can be written in the following linear form: [72]

$$\frac{C_e}{q_e} = \frac{1}{q_m K_L} + \frac{C_e}{q_m} \quad (2.3)$$

Freundlich model

Freundlich model, presented in 1924, is used to describe adsorption processes that occur at heterogenous surfaces [76]. The Freundlich isotherm expression that describes the surface heterogeneity and the non-ideal, reversible adsorption that can be applied to a multilayer adsorption [77]. Equation 2.4 illustrates the Freundlich general equation.

$$q_e = K_F C_e^{\frac{1}{n}} \quad (2.4)$$

where K_F is the adsorption capacity and $1/n$ is the adsorption intensity, and it also represents the heterogeneity of the adsorbate sites and the variable distribution of energy [72]. Additionally, the linear equation (2.5) for the adsorption isotherm is the following.

$$\ln q_e = \ln K_F + \frac{1}{n} \ln C_e \quad (2.5)$$

Redlich-Peterson model

The Redlich-Peterson model is based on an empirical adsorption isotherm equation that combines the Langmuir and Freundlich parameters to fit the adsorption equilibrium, providing a better accuracy than the other ones [72]. The model can be applied to homogeneous and heterogeneous systems, since it is a mix of them and for that no follow ideal monolayer adsorption [78]. The Redlich-Peterson isotherm equation (2.6) is describes as

follows.

$$q_e = \frac{K_{RP}C_e}{1 + \alpha C_e^\beta} \quad (2.6)$$

where K_{RP} is the Redlich-Peterson isotherm constant ($L g^{-1}$), α is a constant ($L mg^{-1}$), and β is an exponent that lies between 0 and 1. When β is equal to 1, the expression reduces to the Langmuir equation with α being the Langmuir adsorption constant (K_L) which is related to the adsorption energy [72]. Additionally, the Redlich-Peterson isotherm linear equation (2.7) can be expressed as follows [79].

$$\frac{C_e}{q_e} = \beta \ln C_e - \ln K_{RP} \quad (2.7)$$

2.3.2 Adsorption kinetics

The adsorption kinetics study is crucial before the application of an adsorbent, helping to obtain optimum parameters, the residence time, and even dimensions for continuous flow processes [80]. During the kinetic study, the aim is to determine the rate of the adsorption process, establishing the rate law for this process through appropriate mathematical expressions that fit the obtained experimental data. Additionally, the kinetic adsorption study can provide insights into the adsorption mechanism, which can vary between different adsorbents and adsorbates, and it is also influenced by the conditions of the system [81]. Kinetics study can provide details on the adsorption mechanism and the steps that affect the rate, such as mass transfer or chemical reactions [82]. Adsorption kinetic models are currently used to analyze the kinetic data behavior. Two of these models are the pseudo-first-order (PFO) and the pseudo-second-order (PSO). Each model is related to mechanisms that explain the type of adsorbate-adsorbent interaction, which are: physisorption, for the PFO model, and chemisorption, for the PSO model [4].

Pseudo-First-Order kinetic model

The Lagergren pseudo-first-order model, which is commonly applied over the initial stage of an adsorption process, is based on the presumption that the rate of change in solute uptake with time is directly proportional to the difference in saturation concentration and the amount of solid uptake with time [83]. The linear differential form of the pseudo-first-

order model can be expressed as follows:

$$\frac{dq_t}{dt} = k_1(q_e - q_t) \quad (2.8)$$

where k_1 is the equilibrium rate constant in the PFO model (L/min), and q_e and q_t (mg/g) are the amounts adsorbed at equilibrium and at time t , respectively [71]. And after integrating Equation 2.8 at the boundary conditions ($t = 0, q_t = 0$ and $t = t, q_e = q_t$), the following linear equation is obtained [84]:

$$\ln(q_e - q_t) = \ln q_e - k_1 t \quad (2.9)$$

And rearranging Equation 2.9, the expression of a non-linear equation is obtained:

$$q_t = q_e(1 - e^{-k_1 t}) \quad (2.10)$$

Pseudo-Second-Order kinetic model

The pseudo-second-order model is based on the assumption of the active sites on the absorbent are finite and a deciding parameter in the increase of the rate of adsorption, which can be described as chemisorption behavior [85]. Therefore, the adsorption capacity of the material is directly related to the adsorption rate with no influence by the concentration of the adsorbate [86]. The differential form for the pseudo-second-order kinetic is expressed as follows:

$$\frac{dq_t}{dt} = k_2(q_e - q_t)^2 \quad (2.11)$$

where k_2 is the equilibrium rate constant in the PSO model. After the integration of Equation 2.11 using the boundary conditions ($t = 0, q_t = 0$ and $t = t, q_e = q_t$), the PSO model equation can be expressed as the Equation 2.12 [84].

$$q_t = \frac{q_e^2 k_2 t}{q_e k_2 t + 1} \quad (2.12)$$

And finally, Equation 2.12 can be rearranged to obtain the linear equation (Equation 2.13):

$$\frac{1}{q_t} = \left(\frac{1}{k_2 q_e^2}\right) \frac{1}{t} + \frac{1}{q_e} \quad (2.13)$$

2.3.3 Adsorption thermodynamics

For a better understanding of how temperature affects the adsorption process and to determine whether events occur spontaneously or not, the study of thermodynamic parameters is crucial [87]. During the adsorption process, parameters such as the Gibbs free energy (ΔG°), enthalpy (ΔH°), and entropy (ΔS°) change can be determined. For ΔH° and ΔS° , their values can be estimated by the Van't Hoff equation (2.15) representation as $\ln K^\circ$ versus $1/T$. While ΔG° estimation is through the evaluation of Equation 2.14 at each absolute temperature [88].

$$\Delta G^\circ = -RT \ln K^\circ \quad (2.14)$$

$$\ln K^\circ = \frac{-\Delta H^\circ}{RT} + \frac{\Delta S^\circ}{R} \quad (2.15)$$

where R (8.314 J/mol K) is the universal gas constant, K° is the standard equilibrium constant, and T (K) is the absolute temperature of the solution.

Langmuir isotherm method

As it was aforementioned in the Langmuir equation (Equation 2.2) K_L is the equilibrium constant representing the ratio of adsorption rate versus the ratio of desorption rate [89]. Although, K_L cannot be the standard equilibrium constant, since their units are the reciprocal to the solute concentration [90]. So a suitable method to calculate the standard equilibrium constant was proposed by Zhou et al., providing the following equation from the Langmuir one [91]:

$$\Theta = \frac{K^\circ \frac{C_e}{C^\circ}}{1 + K^\circ \frac{C_e}{C^\circ}} \quad (2.16)$$

where Θ is the fraction of the surface covered at equilibrium, C_e is the equilibrium concentration of solute (mg/L), and C° is the concentration of the solution in the chosen standard state, $C^\circ = 1$ mol/L (or the equivalent in the adsorbed compound for mg/L units).

Chapter 3

Methodology

3.1 Materials and Reagents

The reagents used in this work were supplied from

- Sigma Aldrich: Citric acid (Ca), Acetic acid (liquid 99.5%), Potassium dichromate $K_2Cr_2O_4$ (99.5%)
- Biofitness: Chitosan (Ch)

On the other hand, to carry out the characterization techniques, this work employed the following laboratory equipment:

- Fourier Transform Infrared Spectroscopy (FTIR)
- Thermogravimetric Analyzer (TGA)
- Scanning Electron Microscopy (SEM)
- Atomic Absorption Spectroscopy (AAS)
- UV-Vis Absorption Spectroscopy (UV-Vis)

3.2 Aerogels Synthesis

The synthesis method in the current thesis project is based on the Ponnusamy et al. work with varied modifications [92], using a more accessible material such as citric acid as the

crosslinking agent. A 2% chitosan solution was prepared in a 2% acetic aqueous solution. Then, the citric acid was slowly added to the solution at 80 °C for 15 minutes, under magnetic stirring, to induce the crosslinking. The solution is cold in a plastic vessel for 1 hour, and put in a super refrigerator for 24 hours, to achieve -80 °C. The freeze solution is rested in a fume hood until a hydrogel consistency is obtained, it only occurs at specific citric acid-chitosan ratios. The hydrogel is kept at -80 °C for 24 hours and then lyophilized for 48 hours. The result aerogel is vacuum dried at 30 °C for 48 hours to remove the remaining acetic acid. The nomenclature and composition of the resulting aerogels are described in Table 3.1, where the measured raw materials are expressed for 50 mL of solution.

Table 3.1: Nomenclature of the different synthesized aerogels and their weighted raw materials.

Nomenclature	Chitosan (g)	Citric acid (g)
ChModel	1	0
Ch5Ca1	1	0.2
Ch3Ca1	1	0.33
Ch2Ca1	1	0.5
Ch1Ca1	1	1

For the characterization part of the chitosan aerogels via ATR-FTIR, TGA, swelling experiment, and adsorption studies, all the mentioned samples were tested. Distilled water was employed for the swelling experiment, while potassium dichromate $K_2Cr_2O_4$ (99%) solutions were used in the adsorption studies.

3.3 Aerogels characterization

3.3.1 Fourier transform infrared spectroscopy (FTIR)

Attended total reflectance - Fourier transform infrared (ATR-FTIR) spectroscopy was employed to illustrate the chemical structure and evaluate functional groups present on the surface of the chitosan aerogels. All the samples (ChModel, Ch5Ca1, Ch3Ca1, Ch2Ca1, and Ch1Ca1) were examined in the wide range of the infrared region between 400 cm^{-1} to 4000 cm^{-1} using the attenuated total reflectance (ATR) sampling technique in the Cary

630 FT-IR Spectrometer. Additionally, a citric acid sample was tested in a specific range near 1705 cm^{-1} (1600 to 1800 cm^{-1}).

3.3.2 Thermogravimetric analysis (TGA)

Thermogravimetric analysis is a technique in which the weight of a sample material is continuously measured under a controlled atmosphere and temperature program. Additionally, this data can be interpreted as the variation of sample weight with respect to temperature or time, and the differential thermogravimetric (DTG) curve obtained [93]. For this work, all synthesized aerogels were analyzed to evaluate their cross-linking degree by the variation of their physical and chemical properties. The general specifications for the analysis were a range temperature of 20 to $700\text{ }^{\circ}\text{C}$ and a temperature rate of $10\text{ }^{\circ}\text{C}/\text{min}$.

3.3.3 Cr(VI) adsorption analysis

To evaluate which aerogels exhibit the best absorption capacity, Cr(VI) adsorption analyses for each one was performed to remove ions of Cr(VI) from aqueous solutions. The evaluation of the adsorption capacity consisted of quantifying Cr(VI) in a solution before and after the adsorption processes. An Atomic absorption spectrometer (AAS) was used to measure the concentration of Cr(VI), which was indirectly calculated by Equation 3.1.

$$\%Removal = \frac{(C_i - C_e)}{C_i} * 100 \quad (3.1)$$

where C_i and C_e correspond to the initial and equilibrium concentrations of the Cr(VI) solutions, respectively, in mg/L.

3.3.4 Scanning Electron Microscopy (SEM)

Scanning Electron Microscope (SEM) is a microscope designed for studying the surfaces of solid materials, that uses electrons of low energy to produce high-resolution images with a three-dimensional appearance [94]. This instrument can illustrate the surface structure of the analyzing material. In this work, images of the aerogel were obtained from the interactions with an electron beam focused on observing the surface morphology and porosity.

3.4 Swelling Of Chitosan Aerogels

Aerogels have a high surface area which provides them the capacity to retain a significant fraction of water in their structure. The aerogels' swelling degree was determined by getting the weight after and before the swelling process, in which three identical samples were submerged during a specific time in distilled water. The general conditions of distilled water were a temperature of 20 °C and a pH of 6. By repeating the process at different time intervals, the swelling rate is measured. The submerged aerogels were extracted at a specific time interval, and let drain the excess water on the vessel wall was for 3 seconds, subsequently weighing the swollen samples. The swelling percentage was calculated by Equation 3.2.

$$E_{sr}(\%) = \frac{(W_s - W_d)}{W_d} * 100 \quad (3.2)$$

where E_{sr} is related to the water absorption percentage of the aerogels, and W_d and W_s are the dry and swollen weights of the samples respectively.

3.5 Adsorption evaluation

For the absorption evaluation, a series of absorption experiments were developed to analyze the effects of the involved variables in the process such as the temperature of the solution and contact time, all the experiments were conducted on the aerogel which presented the highest Cr(VI) adsorption capacity. The main stages for the evaluation were the construction of the calibration curve and the analysis of the absorption kinetic and adsorption isotherms. For each stage, the atomic absorption spectrometer and the UV-Vis absorption spectrometer were used to calculate the concentrations of the Cr(VI) solutions. Both methods were used due to the limitations on the range concentration, which can be fixed by working with the best equipment at a concentration interval.

3.5.1 Calibration curve

First, it was necessary to calculate the concentration range in which is working and split it into some intervals where the behavior is almost linear. For this work, the following intervals were estimated: 0.01-0.1 mg/L, 0.1-1 mg/L, 1-10 mg/L, and 10-100 mg/L, in

order to keep the linearity of the data and with a maximum of 100 mg/L, since it is the average Cr(VI) concentration from the tanning process wastewater in Ecuador. For almost all the ranges the atomic absorption spectrometer was used, the only exception was the interval 10-100 mg/L where the UV-Vis absorption spectrometer was used. On the other hand, a mother solution of 1000 mg/L was prepared using the potassium dichromate $K_2Cr_2O_4$ powder and distilled water. Then, smaller dissolves were prepared for each interval, and the solutions sample prepared was 1-liter volume. All the prepared solutions' absorbance was measured using the aforementioned equipment, and for the UV-Vis absorption spectroscopy, the measure was in a wavelength of 349 nm. Finally using all absorbent measurements, the calibration curve was built by applying the Lambert-beer law, which equation is the following [95]:

$$A = \varepsilon Cl \quad (3.3)$$

where A is the absorbance, ε is the adsorption coefficient, C is the concentration, and l is the optical path length.

3.5.2 Adsorption kinetic

The kinetic adsorption study is the evaluation of the adsorption process during a given time interval under constant temperature conditions. This analysis may be a measure of the diffusion of the chromium ions through the aerogel structure [71], which allows for predicting the rate of Cr(VI) removal from aqueous solutions by the aerogel. For the evaluation of the adsorption process of the aerogel, a series of experiences were conducted on the selected aerogel. Kinetic tests were carried out with general specifications for the procedure: a proportion of 20 mg adsorbent to 50 mL of a Cr(VI) solution of 10 mg/L at room temperature with continuous stirring. The test duration was varied according to the obtained previous results to finally collect data for 3, 7, 15, 25, 40, 50, 75, 90, and 120 minutes since in this range was appreciated the most significant variations of concentration. A sample of each final solution was collected and filtrated to evaluate their concentration by the atomic absorption spectrometer. Finally, Equation 3.4 was used to determine the

absorption capacity at that time period.

$$q_t = \frac{(C_i - C_t) * V}{W} \quad (3.4)$$

where q_t refers to the amount of Cr(VI) adsorbed on the aerogel at a time interval expressed in mg/g, while C_i and C_t correspond to the initial and final concentrations, in mg/L, of Cr(VI) solutions respectively, finally V is the volume of solution and W is the weight of the adsorbent, in mL and mg respectively.

3.5.3 Adsorption isotherms

From the prepared solutions for the calibration curve samples of 50 ml were collected to produce the experiences, the concentrations employed were 1, 2, 3, 4, 5, 6, 8, 10, 20, 30, 40, 50, 60, 70, 80, 90 mg/L of Cr(VI), selected due to the noticed tendency as the experience was made. For the absorption the specifications were a proportion of 20 mg adsorbent to 50 mL of a Cr(VI) solution of 10 mg/L at room temperature with continuous stirring for 24 hours. For stirring, an orbital shaker was used. Samples of each solution were obtained and filtrated, then analyzed by atomic absorption spectroscopy or UV-Vis absorbance spectroscopy. Then, Equation 3.5 was used to determine the absorption capacity at equilibrium.

$$q_e = \frac{(C_i - C_e) * V}{W} \quad (3.5)$$

where q_e refers to the amount of Cr(VI) adsorbed on the aerogel expressed in mg/g, while C_i and C_e correspond to the initial and equilibrium concentrations, in mg/L, of Cr(VI) solutions respectively, finally V is the volume of solution and W is the weight of the adsorbent, in mL and mg respectively. Finally, the procedure was repeated using an atmosphere control orbital shaker at 30 and 37 °C temperatures. This data is used to evaluate the thermodynamic behavior of the aerogel and to analyze the adsorption immobilization method. To sum up the employed methodology, Figure 3.1 illustrates the steps followed for the analysis of the aerogels.

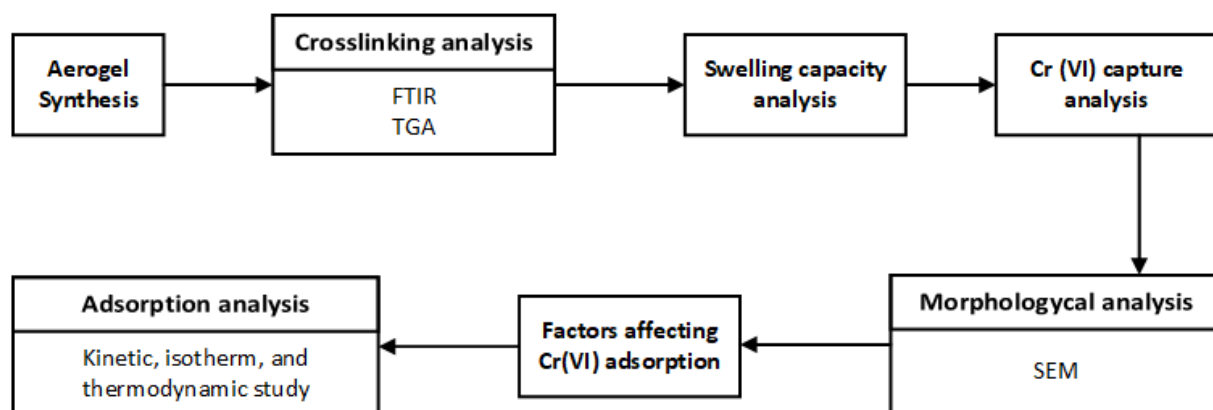


Figure 3.1: Block diagram representation of the methodology followed for the study.

Chapter 4

Results and Discussion

4.1 Synthesis analysis

As it was aforementioned for the synthesis a solution of 2% chitosan was prepared from 2% acetic acid; the final solution consistency is appreciated in Figure 4.1.

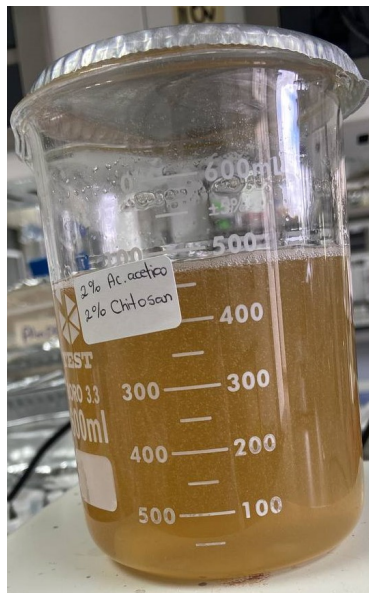


Figure 4.1: Image of the 2% chitosan solution.

Then the citric acid is added according to Table 3.1; in Figure 4.2 is observed the mixture under stirring and 80°C temperature conditions.

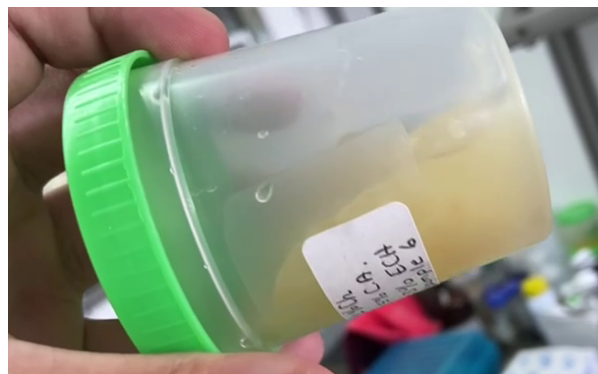


Figure 4.2: Image of the 2% chitosan solution.

Then the solutions are poured in plastic vessels, to cooled at -80°C . After around 24 hours, the freeze solution vessels are rested in a fume hood to obtain the hydrogel consistency. In Figure 4.3 is observed the final hydrogel viscosity, which means the molecules are interacting with each other.



(a)



(b)

Figure 4.3: Images of the hydrogel consistency achieved after the cooling process.

Finally, the hydrogel is cooled again at -80°C , and after around 24 hours the freeze material is lyophilized (Figure 4.4) to obtain the aerogel. The aerogel seems to be like a rigid sponge with a highly porosity.



Figure 4.4: Image of the lyophilization process.

4.2 Crosslinking analysis

4.2.1 Fourier transform infrared spectroscopy (FTIR) analysis

Fourier Transform Infrared Spectroscopy analysis was studied to determine the presence of an interaction between chitosan and citric acid on the chitosan aerogel, due to this technique evaluate the chemical structure of the aerogel by determining the functional groups on their surface.

Figure 4.5 shows the FITR spectra of ChModel, Ch1Ca1, Ch2Ca1, Ch3Ca1, and Ch5Ca1. After analyzing the spectra can be determined the typical peaks for chitosan easily. The peaks above 3000 cm^{-1} particularly $3347 - 3065\text{ cm}^{-1}$ are the -OH stretching vibration superimposed to N-H stretching. Another peak observed in $2917 - 1873\text{ cm}^{-1}$ belongs to aliphatic C-H stretching. [96] The typical peaks in 1660 (C=O stretching of C=O-NHR group) and 1598 cm^{-1} (NH_2 deformation) seem to be moved to 1628 and 1532 cm^{-1} by the presence of the acetic acid during the aerogel forming structure, now being an NH^{3+} group [64]. The peaks at 1150 and 1062 cm^{-1} , which correspond to the glycosidic bonds of the skeletal polysaccharides, were related to the stretching of the asymmetric C-O bond and the vibration of the C-O-C bridge in the ring and β -glycosidic bond respectively, reporting similar peak to those reported by Bosquez et al. [97]. Additionally, minor peaks such as 1396 (N-H vibrations in primary amines) and 893 cm^{-1} (ring stretching) [98].

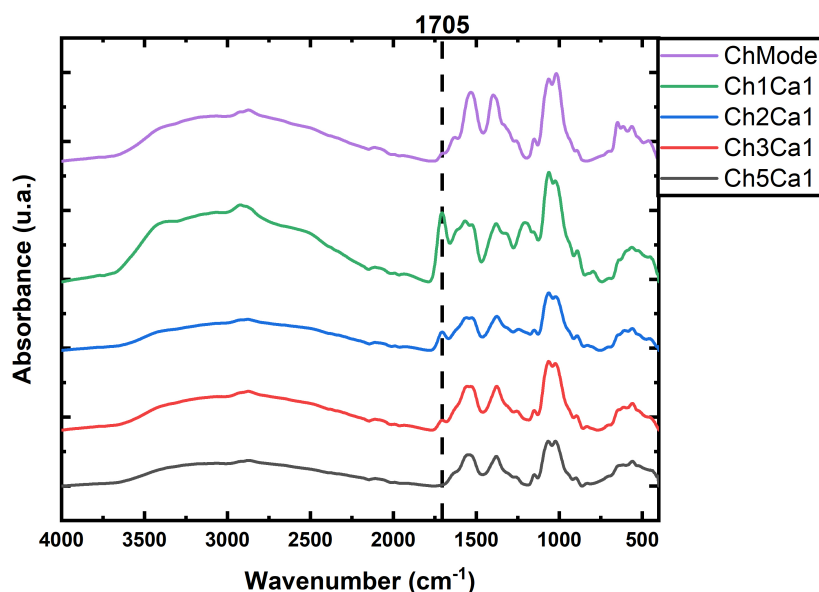


Figure 4.5: Comparison of FTIR graphs of the synthesized chitosan aerogels in the range of 4000 to 400 cm^{-1} .

A particular peak in 1705 cm^{-1} appears as the citric acid fraction increase. For the analysis of the particular peak, figure 4.6 shows the FTIR spectra of Ch1Ca1, Ch2Ca1, Ch3Ca1, Ch5Ca1, and citric acid in the interval of 1600 - 1800 cm^{-1} . It is noticed that the double peak of 1743 - 1692 cm^{-1} arises to C=O stretch in the carboxylic groups, which is not visible in the chitosan aerogels [99]. The unique peak at 1705 cm^{-1} suggested the physical crosslinking between the amine and the carboxylic group [66], as is illustrated in Figure 2.3. The chemical crosslinking is not possible to observe by this technique because the amide group (form in the covalent bond) is already present in the chitosan structure at some level.

4.2.2 Thermogravimetric analysis (TGA)

Thermogravimetric analysis (TGA) is used as a supporting material to determine the cross-linking grade. This technique consists of controlling the atmosphere temperature of a sample and measuring its weight as a response, it can be expressed in a plot with an independent variable of temperature or time (knowing the temperature increase rate). For this project, the conditions were a range temperature of between 20 to 700 °C (standard

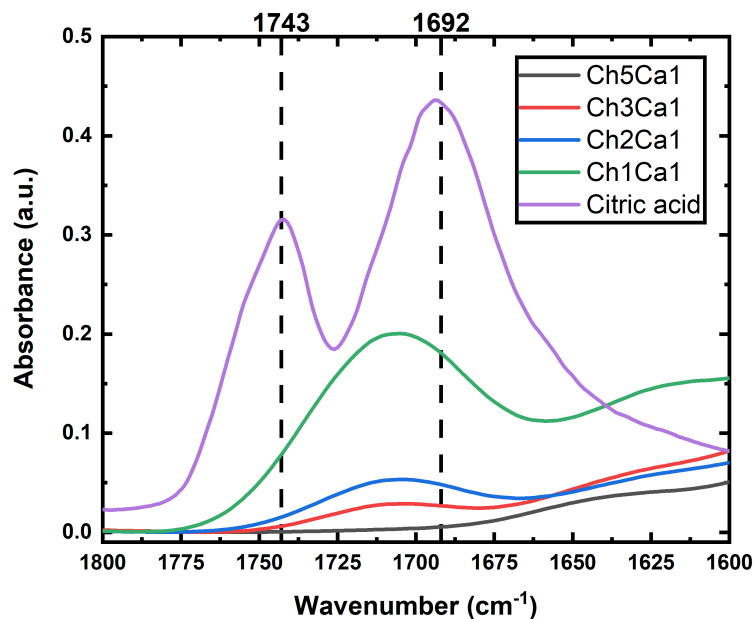


Figure 4.6: Comparison of FTIR graphs between the synthesized chitosan aerogels and citric acid powder in the range of 1800 to 1600 cm^{-1} .

range for biopolymers) and a temperature rate of 10 °C/min. Figure 4.7 illustrates the TGA plots of pure chitosan and Ch1Ca1, Ch2Ca1, Ch3Ca1, and Ch5Ca1 aerogels. It is noticed that as temperature increases the measured weight starts to decrease; for pure chitosan is visible that the associated temperature is 300 °C, which according to the literature is its degradation temperature [100]. Otherwise, the chitosan aerogel samples experience an irregular degradation, which is explained by the interference of citric acid in the structure. Additionally, it is observed that in the aerogels samples, degradation starts early near 175 °C of temperature, and in literature, the citric acid degradation temperature is 175 °C [101].

Derivative thermogravimetric analysis is visualized in Figure 4.8, and is noticeable that as the citric acid fraction increases the peak associated with chitosan moved to higher temperatures. This indicates there is a change in the chitosan structure, confirming the cross-linking effect of the citric acid. Another factor is the presence of new peaks in the temperature range of 175 to 250 °C, these are linked to citric acid degradation temperature. But Ch5Ca1, Ch3Ca1, and Ch2Ca1 only have a prominence peak around 225 °C, evidencing

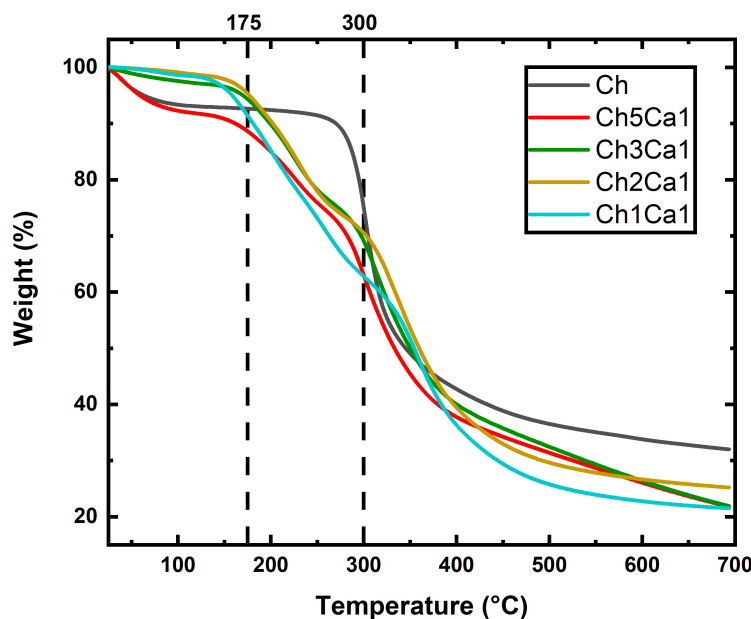


Figure 4.7: Comparison of Thermogravimetric analysis (TGA) plots of the synthesized chitosan aerogels.

the cross-linking between the chitosan and the citric acid. It is appreciable that Ch1Ca1 has three prominence peaks, one of them being at 175 °C which suggested the presence of no-linked citric acid [102].

4.3 Swelling capacity analysis

One of the most important characteristics that aerogels have is the swelling capacity due to their three-dimensional structure, which is associated with the degree of cross-linking, either chemical or physical. The swelling capacity of the aerogel indicates its ability to respond in contact with a liquid, and how slight changes in the liquid components can stimulate the aerogel surface area. For this project, as chitosan is a hydrophilic bio-polymer tends to increase its volume in contact with water, and if we increase the cross-linking degree this property is attenuated [103].

For the experience ChModel, Ch1Ca1, Ch2Ca1, Ch3Ca1, and Ch5Ca1 samples were tested in distilled water (pH~6) and at 20 °C for a varied intervals of time, but when ChModel

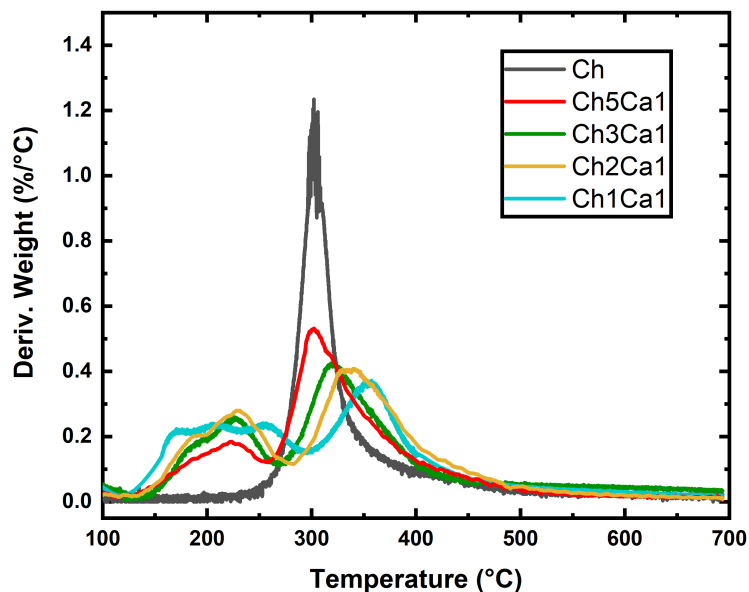


Figure 4.8: Comparison of Derivate thermogravimetric (DTA) plots of the synthesized chitosan aerogels.

and Ch1Ca1 samples get in contact with water they dissolved. The swelling degree for the rest of the samples was obtained by the alteration in weight visualized by the amount of water absorbed. When the prepared aerogels were evaluated a change in color and an increase in volume was visible, the volume augment is directly related to the amount of fluid that the aerogel can uptake in its structure. The swelling capacity was determined by Equation 3.2 and expressed in percentage.

Figure 4.9 shows the swelling kinetics and the behavior of the chitosan aerogels in time. The primary observation of the plot is the quickness with which the aerogels get into the maximum fluid intake, it just takes less than 4 seconds to achieve it. Furthermore, their swollen capacity is above sixteen times their own weight which indicates that it is a good material for sorption activities. Finally, it is noticed that as the citric acid fraction is decreased the swelling degree is increased, it is totally following the expected behavior, since as the citric acid fraction decreases the cross-linking degree increases, and for the aforementioned facts it produces a small place for the fluid intake. A better swelling degree is better for sorption but it must be controlled since it can lead to a material too soft and

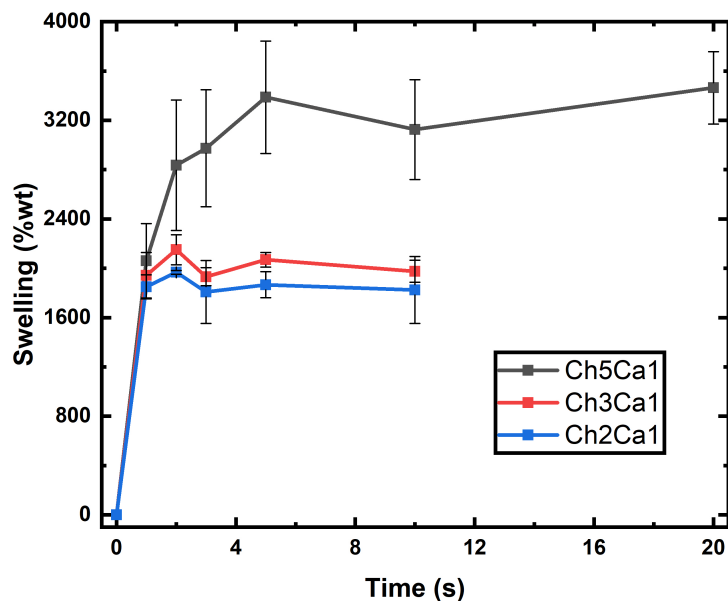


Figure 4.9: Swelling kinetic plots of the Ch5Ca1, Ch3Ca1 & Ch2Ca1 synthesized chitosan aerogels.

easily destructible.

4.4 Chitosan aerogel selection

The selection of the optimal aerogel was based on the capacity to remove the chromium (VI). For the experience a sample of 10 mg of each aerogel (Ch5Ca1, Ch3Ca1, and Ch2Ca1) was put in contact with 25 mL of 5 mg/L Cr(VI) solution under stirring. After at least 20 hours, the samples were extracted and filtered to then estimate the percentage of removal by using Equation 3.1. In Figure 4.10 we can observe how are the changes in appearance and color of the aerogel after the chromium capture, mainly the aerogel with chromium turns yellowish-green.

Additionally, Figure 4.11 compares the removal percentage of the aerogels at the established conditions, and it is appreciated that Ch5Ca1 the one adsorbing the greatest amount of chromium, removing near the 90% of the ions suspended in the solution. This agrees with Ch5Ca1 is the one supporting the greatest amount of liquid in its structure, and

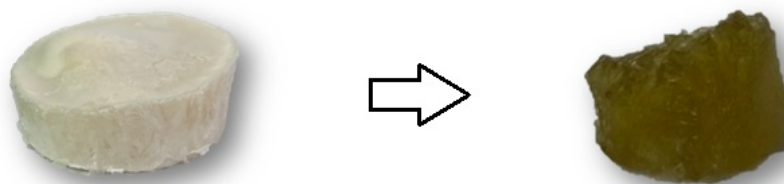


Figure 4.10: Illustration of a chitosan aerogel before and after the Cr(VI) adsorption process.

in fact has a greater surface area and active sites where Cr(VI) ions can adhere. Once selected the aerogel, morphological and adsorption evaluations were carried out for a deeper understanding of the material.

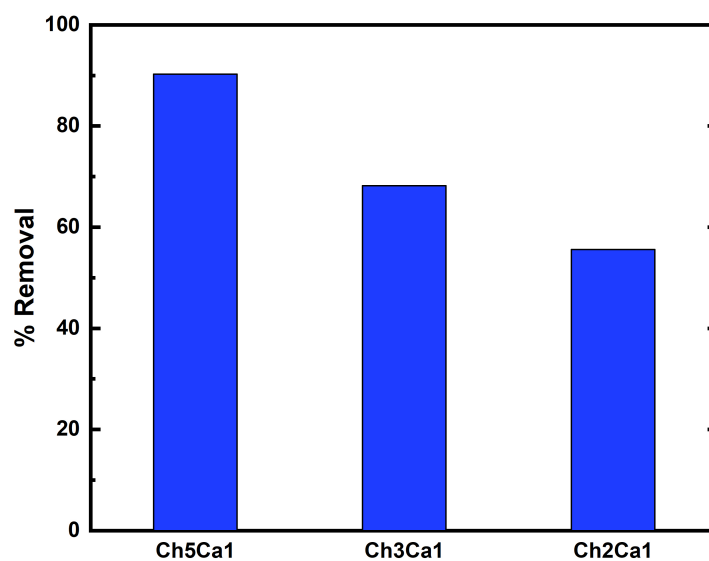


Figure 4.11: Comparison of Cr(VI) adsorption of the Ch5Ca1, Ch3Ca1, and Ch2Ca1 synthesized aerogels in 5 mg/L chromium solutions.

4.5 Morphological analysis

4.5.1 Scanning Electron Microscopy (SEM) analysis

The morphological analysis of the aerogel Ch5Ca1, which was selected according to its capacity to remove chromium from aqueous solutions, it was made by the scanning electron microscopy technique (SEM). These micrographs are illustrated in Figure 4.12 which are in two scales of magnification, the first one in Figure 4.12a of 285x and the second one in Figure 4.12b of 2000x. In Figure 4.12a it is appreciable that the reference bar of 300 μm indicates that the material has irregular macroporosity and also notices a peculiar laminar sheets formation within the structure. Otherwise, Figure 4.12b has a higher resolution with a reference bar of 20 μm , and just a regular pattern of particles is visualized, where is expected to find microporous structures, but due to the instrument limitations, they weren't able to observe. Finally, from the morphological analysis can be inferred that the aerogel has a macroporous structure with laminar paper sheet formations, this agrees with similar materials found in literature [104], and despite the microporous structure isn't clearly observed, it is expected due to the high swollen capacity of the material.

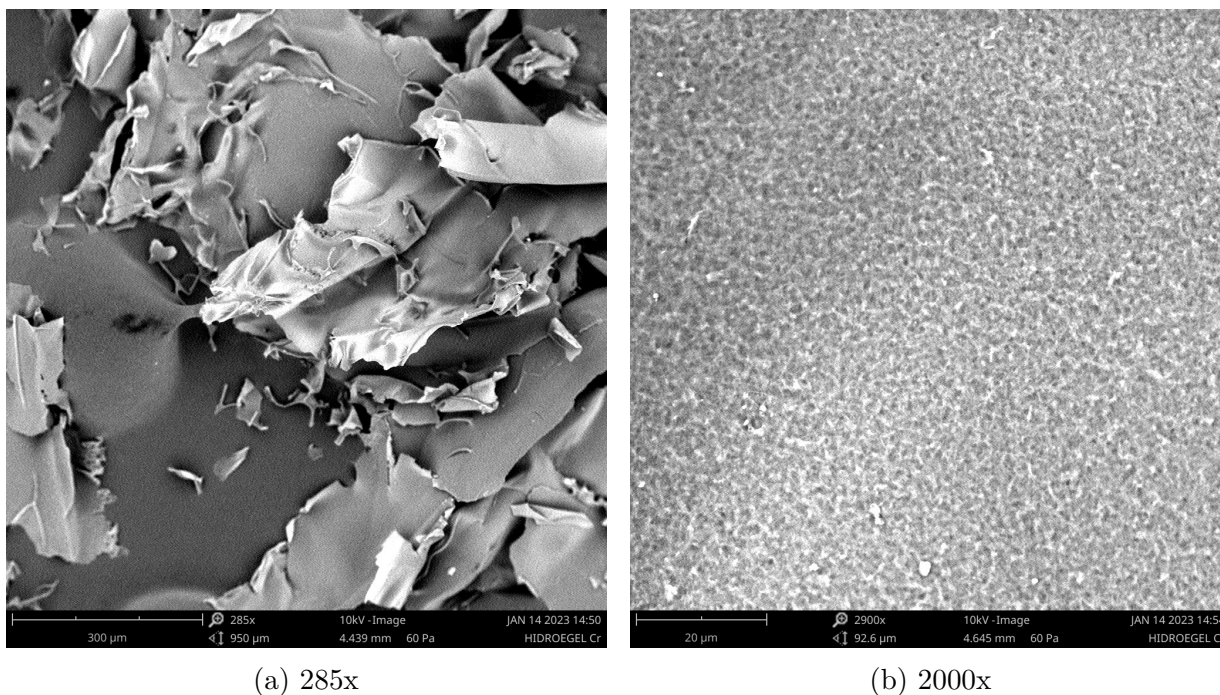


Figure 4.12: Scanning electron microscope images of Ch5Ca1 aerogel at 250x and 2000x

4.6 Adsorption analysis

The adsorption analysis was split into four parts: the adsorption of Cr(VI) experimental parameters that could affect it, Cr(VI) adsorption kinetic study, Cr(VI) adsorption equilibrium study, and Cr(VI) adsorption thermodynamic study.

4.6.1 Factors affecting Cr(VI) adsorption

For the Cr(VI) adsorption analysis several experiments were developed, involving the evaluation of the adsorption capacity under different experimental conditions, in which the parameters of initial concentrations of the Cr(VI) solution, adsorbent dosage (or loading ratio), and temperature were modified.

Effect of initial concentration

To analyze the Cr(VI) solution initial concentration effect, different solutions were prepared with concentrations ranging from 2 to 10 mg/L and then increasing in 10 mg/L until reaching a Cr(VI) solution of 90 mg/L. For all these experiences, 20 mg of Ch5Ca1 aerogels were placed in vessels and 50 mL of each solution was poured on. At 20 °C and under stirring the adsorption process was allowed to occur for about 20 hours to reach equilibrium. Once the equilibrium was reached an aliquot of solution was extracted and filtered. The adsorption capacities (q_e) of the Ch5Ca1 aerogel for the different concentrations of Cr(VI) were determined using the calibration curves constructed previously by applying the Lambert-Beer Law, as well as the aforementioned Equation 3.5. The data obtained from the AAS and UV-Vis spectroscopy measurements of the filtered aliquot of the adsorption system were used for the evaluation.

In Figure 4.13 can be observed the final results for evaluating the Cr(VI) solution initial concentration effect on the adsorption process. where an increase in the adsorption capacity of the Ch5Ca1 aerogel is observed as the initial concentration of Cr(VI) increases too until reaching the maximum capacity around 50 mg/L. For concentrations above 50 mg/L it is noticed that the adsorption capacity remains approximately constant, inferring that at that concentration all the active sites involved in the adsorption have been covered.

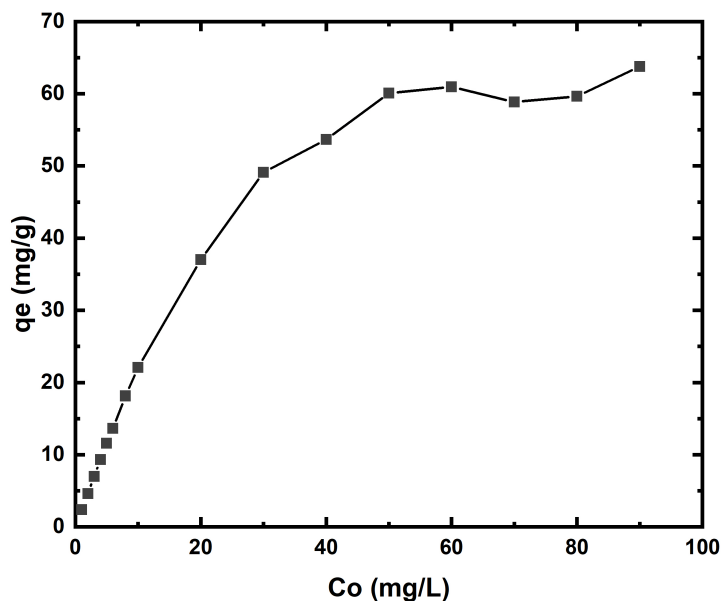


Figure 4.13: Effect of the initial concentration on the Cr(VI) adsorption capacity of the Ch5Ca1 aerogel, for a loading ratio of 20 mg/50 mL at 20 °C.

Effect of adsorbent dosage or loading ratio

For the analysis of the adsorbent dosages effect, experiences at two concentrations (1 and 10 mg/L Cr(VI) solutions) were tested. The different loading ratios evaluated corresponded to 3, 5, 10, 15, 20, 25, 35, 40, 50, and 75 mg. The Cr(VI) adsorption capacity of the Ch5Ca1 samples was tested in batch adsorption, where 50 mL of each Cr(VI) solution was poured into vessels containing samples of the aerogel and were subjected to constant shake for around 20 hours until equilibrium was reached. All charge relationships were evaluated by taking an aliquot of the adsorption system, filtering it, and analyzing it by AAS and UV-Vis spectroscopy. The remaining quantity of chromium in the solution after the adsorption process was determined by Equation 3.5, and the chromium removal percentage was determined by Equation 3.1.

Figure 4.14 illustrates the variation in the removal capacity of the Ch5Ca1 aerogel in dependence on the adsorbent dosage. It is noticed that as the amount of adsorbent increases the greater the percentage of chromium removal until a maximum value is reached. This

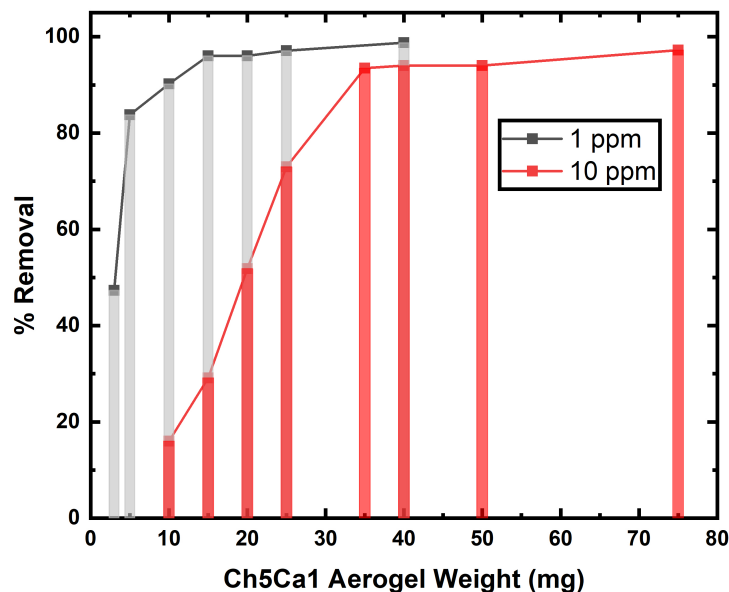


Figure 4.14: Effect of adsorbent weight : adsorbate solution volume ratio (loading ratio) on the adsorption of 50 mL of Cr(VI) solution by Ch5Ca1 aerogel.

trend is observed for both Cr(VI) concentrations tested. The maximum values of removal occur at 15 mg and 35 mg for 1 mg/L and 10 mg/L Cr(VI) solution respectively, being these values the optimal dosage for the highest Cr(VI) removal. Finally, an intermediate value for the adsorbent weight / Cr(VI) solution volume of 20 mg/50 mL was selected for further analysis.

On the other hand, Figure 4.15 illustrates the effect on the adsorption capacity by the variation of the adsorbent dosage. It is appreciated that for both Cr(VI) concentrations, the curves follow an increasing tendency until reaching a maximum where it is supposed that the aerogel has almost adsorbed all the Cr(VI) ions, then the tendency is of decreasing due to the excess of adsorbent used. So, that maximum limit can be considered the maximum adsorption capacity of the material at that specific concentration, and it can also be considered the optimal adsorbent dosage (or loading ratio). Additionally, it is noticed that as the concentration of the solution increases the peak width is widened.

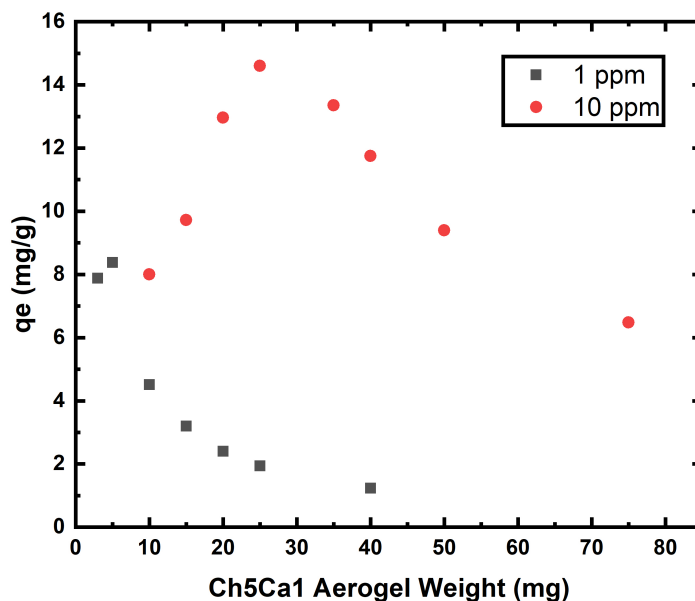


Figure 4.15: Effect of adsorbent weight : adsorbate solution volume ratio (loading ratio) on the adsorption capacity (q_e) of 50 mL of Cr(VI) solution by Ch5Ca1 aerogel. Experimental data plotted at 1 ppm (squares) and 10 ppm (circles) Cr(VI) concentrations.

Effect of temperature

To analyze the effect of temperature, adsorption experiments at 20 °C, 30 °C, and 37 °C were carried out. For the load ratio of 20 mg/ 50 mL, 20 mg of Ch5Ca1 aerogel was poured in 50 mL of 50 mg/L Cr(VI) solution. Through strict temperature control, the batch adsorption experiments were kept under constant agitation by an orbital shaker, for around 20 hours. Once the equilibrium adsorption was achieved, the final solution was evaluated by AAS and UV-Vis spectroscopy measurements, and then the Cr(VI) adsorption capacity was obtained using Equation 3.5. The results are illustrated in the bar diagram shown in Figure 4.16.

From Figure 4.16 is evident that the Cr(VI) adsorption capacity decreases of aerogel with increasing temperature, which means that the higher the temperature, the weaker the interaction between Cr(VI) and the aerogel. The situation favors the Cr(VI) desorption process. While this behavior is consistent with some previous studies [105, 106], there are also reports on materials similar to the one prepared in this study that do not exhibit a

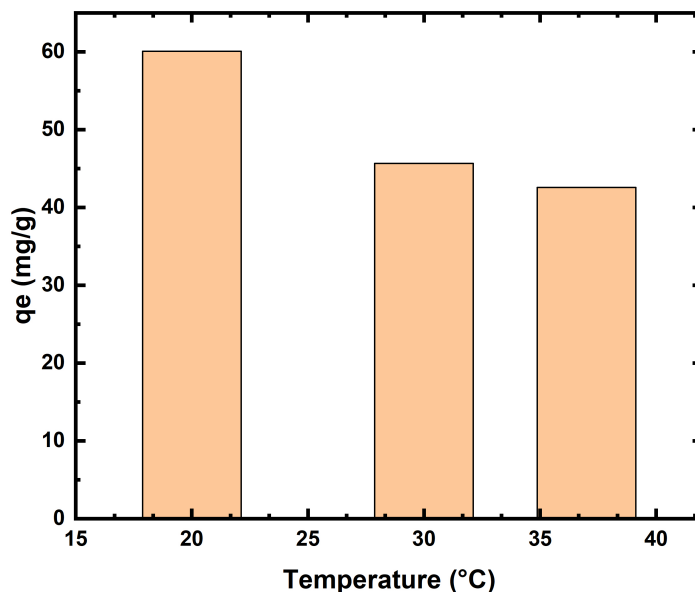


Figure 4.16: Effect of temperature on the Cr(VI) adsorption capacity of the Ch5Ca1 aerogel.

clear trend with changes in temperature [107, 108].

4.6.2 Cr(VI) adsorption kinetic study

For this evaluation, the aerogel with the most favorable behavior against the removal of Cr(VI) in solution, that is Ch5Ca1, was used. The kinetic data were obtained from batch adsorption experiments consisting of the incorporation of a specific amount of Ch5Ca1 aerogel (20 mg) in 50 mL of Cr(VI) solution, in order to maintain the same loading ratio of the previously mentioned studies tested. A solution with an initial concentration of 10 mg/L Cr(VI) was chosen to carry out the kinetic study, due to the equilibrium adsorbed amount of Cr by the Ch5Ca1 aerogel was known from previous experiments. As before, the batch adsorption system was kept under shaking, and the aliquots were taken at different times, i.e., 3, 7, 15, 25, 40, 50, 75, 90, and 120 minutes, for the respective spectroscopic analysis to determine the final concentration for the specified time period. This data was used to calculate the adsorption capacity at different times, using Equation 3.5. Finally, the kinetic data was plotted using the Pseudo-First-Order (PFO) (Equation 2.10) and the Pseudo-Second-Order (PSO) (Equation 2.12) rates equations. Both equations can be also

expressed by their linear forms; Equation 2.9 for the PFO model and Equation 2.13 for the PSO model.

Figure 4.17 illustrates the linear and non-linear fits of the PFO (4.17a) and PSO (4.17b) to the kinetic data (q_t vs t), obtained for the adsorption of 10 mg/L Cr(VI) with a loading ratio of 20 mg/ 50 mL at 20 °C. In Figure 4.17 are shown the respective linear correlation coefficients. It is noticed that the Pseudo-Second-Order (PSO) model better fits the kinetic data, since the correlation coefficient (r^2) is closer to 1 than the one for the Pseudo-First-Order (PFO) model. Additionally, in Table 4.1 are visualized the kinetic parameters and the root-mean-square-error (RMSE) for non-linear fits of both models. The RMSE values are the correlation for the non-linear equations, therefore as the RMSE value is closer to 0 the data has a better approach to the equation. For these fits presented, the PSO with a RMSE value of 0.48, is the model that best represents the behavior of the experimental data.

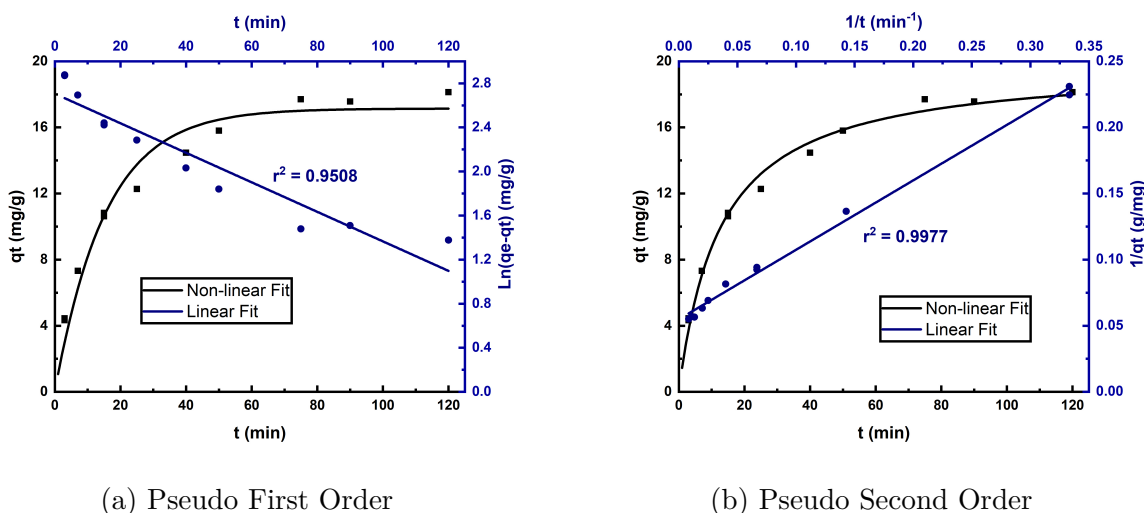


Figure 4.17: PFO (a) and PSO (b) fitted models to data obtained for the adsorption of 10 ppm Cr(VI) with a loading ratio of 20 mg/ 50 mL at 20 °C. Experimental data plotted by both non-linear (squares) and linear (circles) representation model.

The fitting parameter q_e , denoting the equilibrium adsorption capacity, can be compared with the experimental value of 22 mg/g obtained for the case of 10 mg/L Cr (VI) solution, and shown in Figure 4.13. From the information shown in Table 4.1, the value for q_e closer to the experimental one is related to the PSO model, corresponding to a value of 19.88

mg/g. From this information, it can be suggested that the adsorption of chromium ions on Ch5Ca1 aerogel follows a mechanism involving chemical adsorption, due to the PSO model is based on the assumption that the rate-limiting step is the chemical sorption [71]. Finally, assuming that the adsorption kinetic follows the PSO model, the optimal time of the adsorption process to reach a maximum removal of Cr(VI) can be inferred from Figure 4.17b to be 110 min.

Table 4.1: Kinetic adsorption parameters and root-mean-square error (RMSE) for Cr(VI) removal from the PFO and PSO models.

	q_e [mg/g]	k_1 [min ⁻¹]	k_2 [g mg ⁻¹ min ⁻¹]	RMSE
Pseudo First Order	17.14	0.065		1.01
Pseudo Second Order	19.88		3.97	0.48

4.6.3 Cr(VI) adsorption equilibrium study

For the data obtained from adsorption experiments, three isotherm adsorption models were tested, i.e., the Langmuir, Freundlich, and Redlich-Peterson models. Langmuir model principles consider that the adsorption mechanism follows an adsorbate monolayer formation due to the assumption of energetically homogeneous surface sites, for which the adsorption energy is constant [75]. The Freundlich isotherm model assumes a heterogeneous surface, and a multilayer adsorption process is considered, with a non-uniform energy distribution [77]. Finally, the Redlich-Peterson isotherm model combines Langmuir and Freundlich's assumptions for a vast range of concentrations. This model works for both homogeneous and heterogeneous systems, and from the fitting parameter (β), the predominant contribution of the homogeneous or heterogeneous surface to the adsorption process can be inferred [109]. The corresponding descriptive equations isotherms models are above presented in Equations 2.2, 2.4, and 2.6.

The experimental procedure consisted in to pour 20 mg samples of Ch5Ca1 aerogel in 50 mL of 1, 2, 3, 4, 5, 6, 8, 10, 20, 30, 40, 50, 60, 70, 80, 90 mg/L of Cr(VI) solutions to kept the same loading ratio or adsorbent dosage considered in the previous experiment.

The exposition time of aerogel and Cr(VI) solution was around 20 hours for a while a constant temperature and shaking were maintained during the whole experiment. The adsorption experiments were carried out at a pH of around 6 and three temperatures of 20 °C, 30 °C, and 37 °C were tested. The resulting solutions concentrations were estimated from spectroscopic techniques (AAS and UV-Vis). Then, using Equation 3.5, the equilibrium adsorption capacity q_e for each concentration is determined at a specific temperature. The linear and nonlinear trend lines for Langmuir, Freundlich, and Redlich-Peterson models for the isothermal adsorption of Cr(VI) are shown in Figure 4.18, Figure 4.19 and Figure 4.20, respectively.

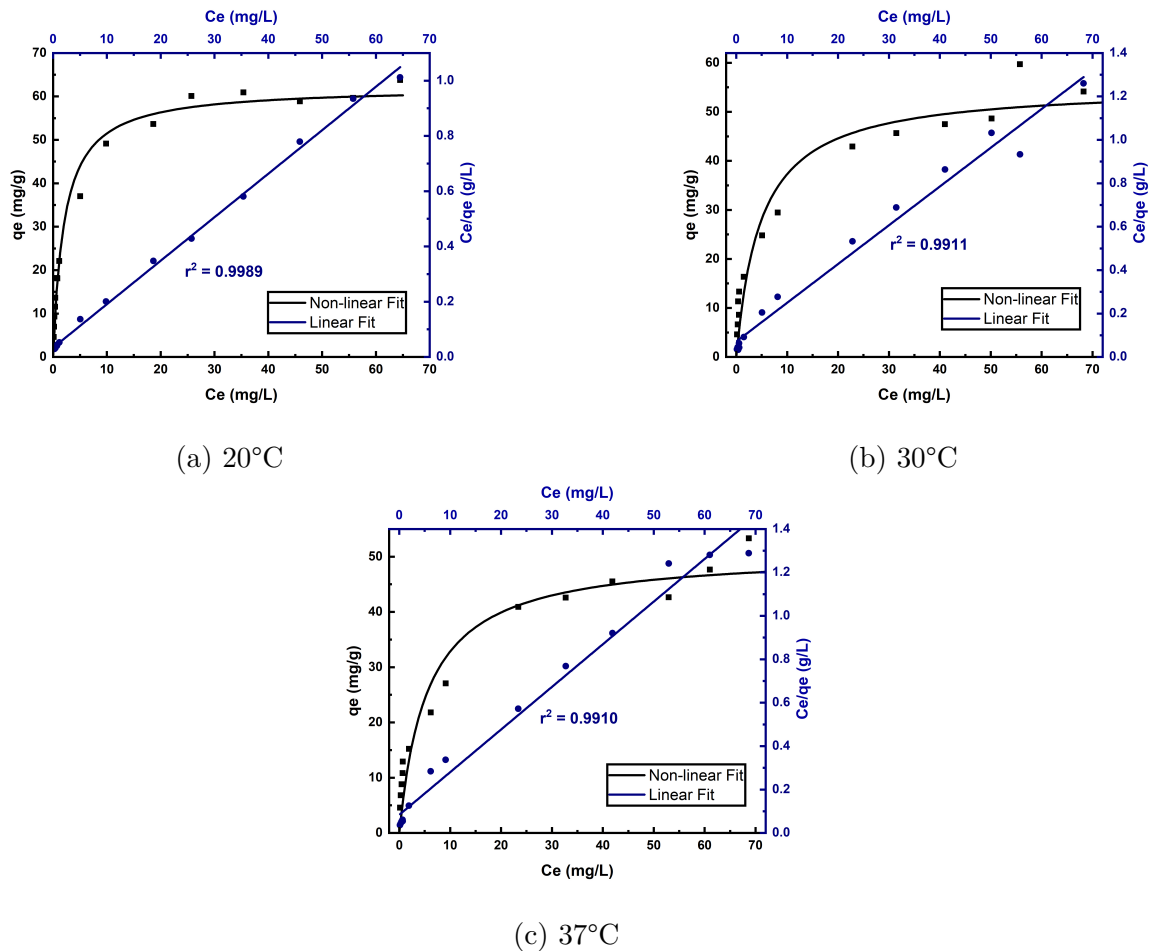


Figure 4.18: Langmuir adsorption isotherm plots for Cr(VI) adsorption by Ch5Ca1 sample at temperatures: 20 (a), 30 (b), 37 °C (c). Experimental data plotted by both non-linear (squares) and linear (circles) representation model.

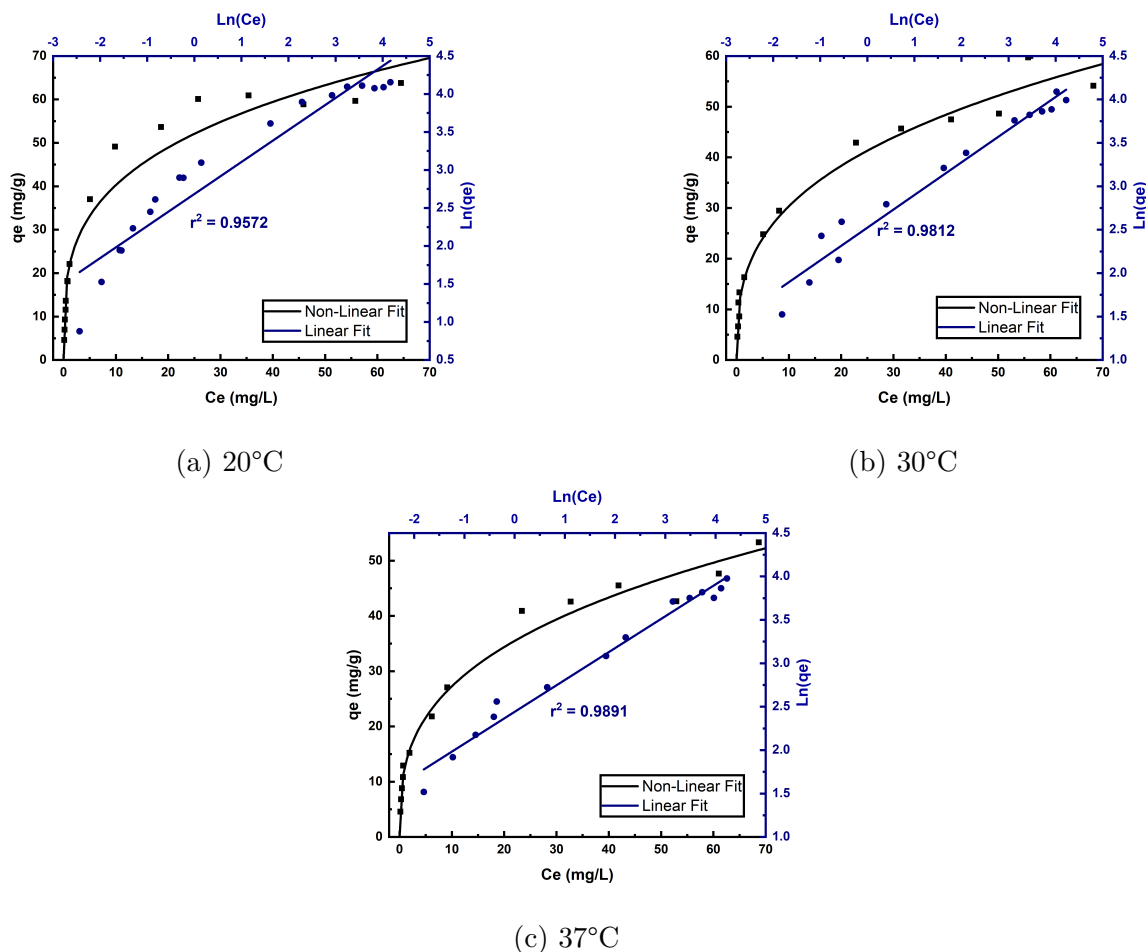
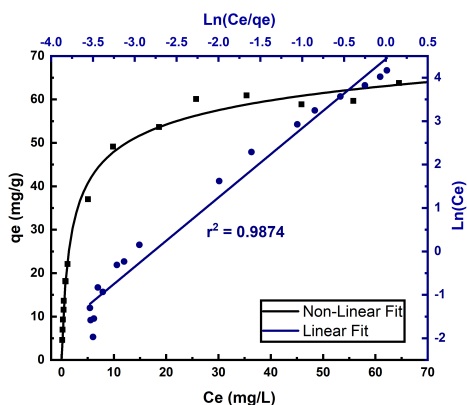
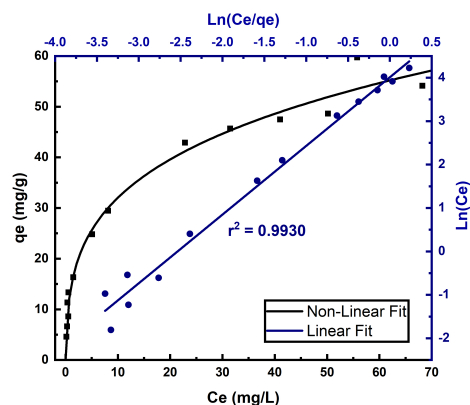


Figure 4.19: Freundlich adsorption isotherm plots for Cr(VI) adsorption by Ch5Ca1 sample at temperatures: 20 (a), 30 (b), 37 °C (c). Experimental data plotted by both non-linear (squares) and linear (circles) representation model.

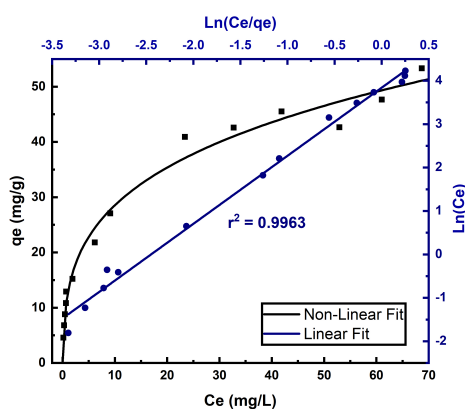
The isotherm model was obtained by two graph editors programs Origin and Excel using Equations 2.3, 2.5, and 2.7, for the linear representation, and Equations 2.2, 2.4, and 2.6 for the non-linear representation estimating the respective correlation coefficients and root-medium-square-error (RMSE). The fittings were made at 20 °C, 30 °C, and 37 °C. Table 4.2 summarizes the calculated isotherm parameters for the Langmuir, Freundlich, and Redlich-Peterson models for the tested temperatures. From the plots illustrated in Figures 4.18, 4.19, and 4.20, temperature dependence of Cr(VI) adsorption on Ch5Ca1 aerogel is confirmed. By comparing of set of plots for each model, that is, 4.18a to 4.18c, 4.19a to 4.19c and 4.20a to 4.20c it can be seen that increases in temperature imply a decrease in the Cr(VI) adsorption capacity of the aerogel. This behavior corroborates that the desorption is favored as the temperature increases, since higher temperature can induce



(a) 20°C



(b) 30°C



(c) 37°C

Figure 4.20: Redlich-Peterson adsorption isotherm plots for Cr(VI) adsorption by Ch5Ca1 sample at temperatures: 20 (a), 30 (b), 37 °C (c). Experimental data plotted by both non-linear (squares) and linear (circles) representation model.

greater mobility of the adsorbate.

Furthermore, comparing the linear correlation coefficients (r^2) obtained for each isotherm adsorption models, it is observed that the value closer to 1 corresponds to the Redlich-Peterson model. Therefore, it is assumed that Redlich-Peterson is the best isotherm adsorption model to represent the behavior of the Ch5Ca1 aerogel for the Cr(VI) adsorption.

The Redlich-Peterson model stands out as the superior choice for describing the adsorption process of Ch5Ca1 aerogel, which is evident from the obtained root-mean-square-error (RMSE) values. The model consistently exhibit smaller RMSE values across all tested temperatures, further reinforcing its predominance. Additionally, the β factor from the

Table 4.2: Adsorption isotherm fitting parameters found from Langmuir, Freundlich, and Redlich-Peterson models at different temperatures for Cr(VI) adsorption by Ch5Ca1 aerogel.

	20 °C	30 °C	37 °C
Langmuir isotherm			
K_L [L/mg]	0.481	0.206	0.182
q_{max} [mg/g]	62.19	55.41	50.84
RMSE	2.524	4.570	4.114
Freundlich isotherm			
K_F [(L/mg) ^{1/n} mg/g]	21.10	13.97	12.62
n	3.562	2.970	2.990
RMSE	5.216	2.667	2.302
Redlich-Peterson isotherm			
K_{RP} [L/g]	40.48	70.11	69.04
α [(L/mg) ^{β}]	0.927	3.977	4.480
β	0.9046	0.7204	0.7141
RMSE	1.706	2.395	2.103

Redlich-Peterson equation lies between 0 and 1 for the three temperatures, this also indicates a good correlation in the model adsorption around the temperature variation [109]. Furthermore, this factor estimates the relation to Langmuir or Freundlich models; if the value is closer to 1 the Langmuir adsorption model behavior predominates over the Freundlich adsorption, and if the value is closer to 0 the opposite occurs [110]. Based on the assumptions, it can be inferred that the adsorption does not follow the ideal monolayer mechanism and combines both homogeneous and heterogeneous adsorption mechanisms, having a slight tendency for the homogeneous one [78]. Additionally, from the data and the analysis can be inferred that the adsorption must be competitive, having a physical and chemical adsorption, which can be attribute to the different functional groups in the chitosan structure.

4.6.4 Cr(VI) adsorption thermodynamic study

For the determination of thermodynamic properties associated with the Cr(VI) adsorption by Ch5Ca1, the experimental data obtained at the different temperatures were used to estimate the values of the equilibrium adsorption constant at each tested temperature. The standard Gibbs free energy (ΔG°) changes for each temperature was estimated from the K°

values according Equation 2.14, which were previously obtained from Langmuir model fit. The dimensionless values for standard equilibrium constant K° were obtained from data given in isotherm studies and Equation 2.16. The data employed in the calculations is the same as in the equilibrium study, and the constants were obtained using the nonlinear fitting making used of appropriate conversion for concentration values. Once K° and ΔG° at each temperature were estimated, the values for the standard enthalpy (ΔH°) and entropy (ΔS°) changes were determined by graphing of Van't Hoof equation given in Equation 2.15. The obtained results for these properties are shown in Table 4.3.

Table 4.3: Thermodynamic equilibrium constants and parameters for Cr(VI) adsorption into Ch5Ca1 samples obtained by Langmuir equation method.

T [K]	LnK	ΔG° [kJ/mol]	ΔH° [kJ/mol]	ΔS° [J/mol K]
293	4.45	-10.84	-23.72	-44.10
303	4.07	-10.24		
310	3.92	-10.11		

Values given in Table 4.3 involve negative values for the standard Gibbs free energy (ΔG°), enthalpy (ΔH°), and entropy (ΔS°) changes at the tested temperatures. For the case of Gibbs free energy (ΔG°), a negative value means the adsorption process is of spontaneous nature, so the process favorably occurs at the tested temperatures, with the tendency to become less negative as the temperature increases. The decrease in adsorption capacity with increasing temperature observed in section 4.6.3 indicates that the adsorption process is exothermic in nature, and it is proven by the negative enthalpy change (ΔH°) value, which indicates that the adsorption process releases energy [10]. Finally, the negative entropy change (ΔS°) value suggests a decrease in the randomness at the Ch5Ca1 aerogel/Cr(VI) ions interface [81], assuming that a higher order in the spatial configuration of the involved species occurs during the adsorption process. A strong interaction between the Cr(VI) ions and the Ch5Ca1 aerogel active sites may be responsible for the decrease in the degree of freedom of the system, which means the capture of Cr(VI) ions hinder the aerogel flexibility and their diffusion in the system [111].

4.7 Economic study

For the economic study was needed to structure the process chain, which can be visualized in Figure 4.21 in a block diagram of the aerogel synthesis. The analysis is superficial and only will focus on the production cost, without the initial supply of the equipment.

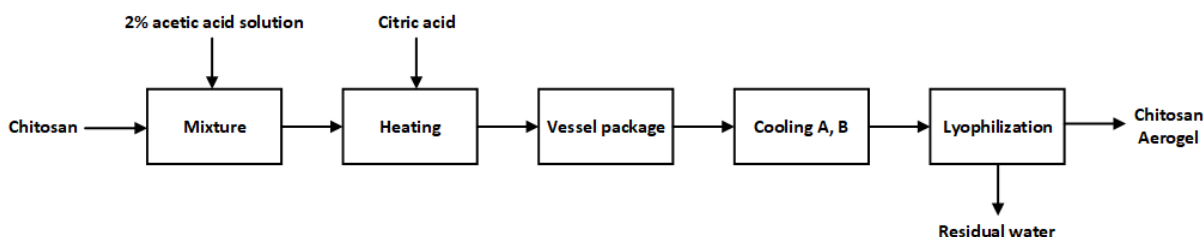


Figure 4.21: Block diagram process for the chitosan aerogel synthesis.

To quantify the aerogel production, the leather production in Ecuador was estimated, which is reported in the literature at 350 M units per year [112]. Additionally, it is reported that each leather production releases around 1000 L of wastewater [113]. Calculating can be said that Ecuador generates 350 MM of wastewater from the leather industry, which contains around 50 mg/L of Cr(VI) concentration [113]. This means that around 14 kg Cr(VI) is in contact with nature annually, and since our material capture capacity is limited to 60 mg/g around 235 tons of aerogel are needed to manage the toxicity. But, a study in Ecuador of chitosan production estimated their capacity at 110 tons with a selling price of around \$ 58/kg [114], and also the market has competitive materials such as active carbon. Therefore, the aerogel production was limited to 150 tons.

For the industrial process the Mixture and Heating unit operations can be carried out in isothermal tanks during a batch reaction, and after the vessels packing the freeze-drying process is enclosed with the cooling and lyophilization unit operations. For the economic analysis, only the freeze-drying process is considered due to the complexity and high price. The raw materials needed for the process are exposed in Table 4.4 with their annual demand and price (250 working days were used for the study); the data for citric and acetic acid was consulted in commercial pages for industrial reagents [115]. It is noticed that chitosan is the material with the higher price. Additionally, compared with the Chinese

price at the industrial scale, which is \$ 10/kg, is greatly superior. So a comparison of the final aerogels price between the two countries was made.

Table 4.4: Raw materials for the synthesis of the aerogels with their annual demand and price.

Raw materials	Annual quantity	Price
Chitosan	125 ton	\$ 7.25 MM
Citric acid	25 ton	\$ 80 M
Acetic acid	62.5 ton m ³	\$ 32.5 M

For the comparison, the price of the freeze-drying process was analyzed, which according to literature estimations the whole process has a consumption of around \$ 10.5/kg produced with a time duration of 3 days [116]. In the present case, it can be quantified as around \$ 1.575 MM. Finally, with the reviewed data, the cost of production of the aerogels can be calculated, obtaining a value of \$ 59.6/kg for the Ecuador price, and a value of \$ 11.6/kg for the China price. So, an internationally, competitive industry is needed in Ecuador to optimize prices and made it possible for aerogels to be competitive adsorbent materials.

Chapter 5

Conclusions

The current project shows the successful preparation of a chitosan-based aerogel cross-linked with citric acid by the sol-gel method using the freeze-dried process. The resulting material turned out to be an efficient adsorbent for the removal of Cr(VI) from aqueous solutions.

FTIR and TGA studies showed that the chitosan was successfully cross-linked by citric acid through interactions between the amino groups from chitosan and the carboxylic groups from citric acid. Furthermore, the cross-linking only occurred in a particular range of chitosan-citric acid ratios between 5:1 to 2:1, and an increase in the cross-linking degree was observed as the citric acid increases. In contrast, lower and higher ratios dissolved completely at water contact. Among the synthesized aerogels, during the Cr(VI) adsorption tests, the optimal adsorption was achieved by the aerogel with the Ch/Ca ratio of 5:1, which has been codified as Ch5Ca1.

Kinetics evaluations determined that the adsorption mechanism fits better with the Pseudo-Second-Order (PSO) model rather than the Pseudo-First-Order (PFO), so the mechanism suggested is chemical adsorption, with an optimal adsorption time of 110 minutes. On the other hand, the isothermal studies fit with the Redlich-Peterson model, which combines Langmuir and Freundlich's models assumptions, indicating the systems are not ideally homogeneous, but more likely a combination of both, with a predominance of a homogeneous surface. The Redlich-Peterson β factor values obtained show a tendency of decreasing with

the temperature increment, suggesting that the homogeneity decreases as temperature increases. Additionally, Langmuir's model maximum adsorption capacity was 62.19 mg/g at 20 °C with a 20 mg aerogel/ 50 mL of Cr(VI) solution ratio. On the other hand, the adsorption mechanism can be interpreted as mixture of chemical and physical adsorption, explained by the different functional groups in the chitosan.

Furthermore, all the calculated thermodynamic properties were negative, which for the Gibbs free energy change (ΔG°) the spontaneity of the process is demonstrated, for the enthalpy change (ΔH°) it suggests that the adsorption process is exothermic. The negative value for the entropy change (ΔS°) suggests the orderliness of the system increases during the adsorption process, involving shows a decrease in the system's degree of freedom, maybe as a result of strong adsorbate-adsorbent interactions.

Finally, the economic study revealed the importance of aerogels research and created an approximation to estimate the production cost of the proposed material, which varies according to the reference value employed for the commercial chitosan, having prices of \$ 59.6/kg for Ecuador's reference and a value of \$ 11.6/kg for China's reference.

As recommendations for future projects, analysis on X-ray photoelectron spectroscopy (XPS) must be implemented to visualize the mechanism of crosslinking. In the thermodynamic analysis, an extension of the tested temperature range is needed to verify the true trend. And, mechanical properties analysis can be made to understand the reusability and resistance of the aerogel.

Bibliography

- [1] S. N. Malik, P. C. Ghosh, A. N. Vaidya, and S. N. Mudliar, “Hybrid ozonation process for industrial wastewater treatment: Principles and applications: A review,” *Journal of Water Process Engineering*, vol. 35, p. 101193, 2020.
- [2] S. Begum, N. Y. Yuhana, N. M. Saleh, N. H. N. Kamarudin, and A. B. Sulong, “Review of chitosan composite as a heavy metal adsorbent: Material preparation and properties,” *Carbohydrate polymers*, vol. 259, p. 117613, 2021.
- [3] Y. Zhang and Y. Shen, “Wastewater irrigation: past, present, and future,” *Wiley Interdisciplinary Reviews: Water*, vol. 6, no. 3, p. e1234, 2019.
- [4] Y. Sheth, S. Dharaskar, M. Khalid, and S. Sonawane, “An environment friendly approach for heavy metal removal from industrial wastewater using chitosan based biosorbent: A review,” *Sustainable Energy Technologies and Assessments*, vol. 43, p. 100951, 2021.
- [5] B. Aftab, Y. S. Ok, J. Cho, and J. Hur, “Targeted removal of organic foulants in landfill leachate in forward osmosis system integrated with biochar/activated carbon treatment,” *Water research*, vol. 160, pp. 217–227, 2019.
- [6] K. Yin, Q. Wang, M. Lv, and L. Chen, “Microorganism remediation strategies towards heavy metals,” *Chemical Engineering Journal*, vol. 360, pp. 1553–1563, 2019.
- [7] I. Cipriani-Avila, J. Molinero, E. Jara-Negrete, M. Barrado, C. Arcos, S. Mafla, F. Custode, G. Vilaña, N. Carpintero, and V. Ochoa-Herrera, “Heavy metal assessment in drinking waters of ecuador: Quito, ibarra and guayaquil,” *Journal of Water and Health*, vol. 18, no. 6, pp. 1050–1064, 2020.

- [8] A. A. Pesantes, E. P. Carpio, T. Vitvar, M. M. M. López, and J. M. Menéndez-Aguado, “A multi-index analysis approach to heavy metal pollution assessment in river sediments in the ponce enríquez area, ecuador,” *Water*, vol. 11, no. 3, p. 590, 2019.
- [9] L. Qu, H. Huang, F. Xia, Y. Liu, R. A. Dahlgren, M. Zhang, and K. Mei, “Risk analysis of heavy metal concentration in surface waters across the rural-urban interface of the wen-rui tang river, china,” *Environmental pollution*, vol. 237, pp. 639–649, 2018.
- [10] R. Saha, R. Nandi, and B. Saha, “Sources and toxicity of hexavalent chromium,” *Journal of Coordination Chemistry*, vol. 64, no. 10, pp. 1782–1806, 2011.
- [11] A. D. Portilla Pozo, “Análisis técnico ambiental del proceso de la curtiduría serrano de la ciudad ambato y diseño de la planta de tratamiento de las aguas residuales,” 2013.
- [12] J. Guertin, “Toxicity and health effects of chromium (all oxidation states),” *Chromium (VI) handbook*, pp. 215–234, 2004.
- [13] S. Li and Q. Zhang, “Risk assessment and seasonal variations of dissolved trace elements and heavy metals in the upper han river, china,” *Journal of hazardous materials*, vol. 181, no. 1-3, pp. 1051–1058, 2010.
- [14] F. Fu and Q. Wang, “Removal of heavy metal ions from wastewaters: a review,” *Journal of environmental management*, vol. 92, no. 3, pp. 407–418, 2011.
- [15] K. C. Kemp, H. Seema, M. Saleh, N. H. Le, K. Mahesh, V. Chandra, and K. S. Kim, “Environmental applications using graphene composites: water remediation and gas adsorption,” *Nanoscale*, vol. 5, no. 8, pp. 3149–3171, 2013.
- [16] Y. Wang, Y. Su, W. Wang, Y. Fang, S. B. Riffat, and F. Jiang, “The advances of polysaccharide-based aerogels: Preparation and potential application,” *Carbohydrate polymers*, vol. 226, p. 115242, 2019.
- [17] K. Kurita, “Chitin and chitosan: functional biopolymers from marine crustaceans,” *Marine biotechnology*, vol. 8, pp. 203–226, 2006.

- [18] M. Rinaudo, "Chitin and chitosan: Properties and applications," *Progress in polymer science*, vol. 31, no. 7, pp. 603–632, 2006.
- [19] T. Anthonsen, S. P. A. ford, I. C. on Chitin, Chitosan, and G. Skjåk-Bræk, "Chitin and chitosan: sources, chemistry, biochemistry, physical properties, and applications," 1989. [Online]. Available: <https://cir.nii.ac.jp/crid/1130000795571867264.bib?lang=en>
- [20] Q. Wang, Y. Tian, L. Kong, J. Zhang, W. Zuo, Y. Li, and G. Cai, "A novel 3d superelastic polyethyleneimine functionalized chitosan aerogels for selective removal of cr (vi) from aqueous solution: performance and mechanisms," *Chemical Engineering Journal*, vol. 425, p. 131722, 2021.
- [21] J. Zhang, Y. Wang, D. Liang, Z. Xiao, Y. Xie, and J. Li, "Sulfhydryl-modified chitosan aerogel for the adsorption of heavy metal ions and organic dyes," *Industrial & Engineering Chemistry Research*, vol. 59, no. 32, pp. 14 531–14 536, 2020.
- [22] J. Luo, C. Fan, Z. Xiao, T. Sun, and X. Zhou, "Novel graphene oxide/carboxymethyl chitosan aerogels via vacuum-assisted self-assembly for heavy metal adsorption capacity," *Colloids and Surfaces A: Physicochemical and Engineering Aspects*, vol. 578, p. 123584, 2019.
- [23] D. Li, X. Tian, Z. Wang, Z. Guan, X. Li, H. Qiao, H. Ke, L. Luo, and Q. Wei, "Multifunctional adsorbent based on metal-organic framework modified bacterial cellulose/chitosan composite aerogel for high efficient removal of heavy metal ion and organic pollutant," *Chemical Engineering Journal*, vol. 383, p. 123127, 2020.
- [24] T. Shahnaz, V. Sharma, S. Subbiah, and S. Narayanasamy, "Multivariate optimisation of cr (vi), co (iii) and cu (ii) adsorption onto nanobentonite incorporated nanocellulose/chitosan aerogel using response surface methodology," *Journal of Water Process Engineering*, vol. 36, p. 101283, 2020.
- [25] R. Verma and P. Dwivedi, "Heavy metal water pollution-a case study," *Recent Research in Science and Technology*, vol. 5, no. 5, 2013.

- [26] B. Baranowska-Dutkiewicz, "Absorption of hexavalent chromium by skin in man," *Archives of toxicology*, vol. 47, pp. 47–50, 1981.
- [27] R. Reza and G. Singh, "Heavy metal contamination and its indexing approach for river water," *International journal of environmental science & technology*, vol. 7, pp. 785–792, 2010.
- [28] B. Sarkar, *Heavy metals in the environment*. CRC press, 2002.
- [29] S. K. Agarwal, *Heavy metal pollution*. APH publishing, 2009, vol. 4.
- [30] P. B. Tchounwou, C. G. Yedjou, A. K. Patlolla, and D. J. Sutton, "Heavy metal toxicity and the environment," *Molecular, clinical and environmental toxicology: volume 3: environmental toxicology*, pp. 133–164, 2012.
- [31] S. J. Hawkes, "What is a "heavy metal"?" *Journal of chemical education*, vol. 74, no. 11, p. 1374, 1997.
- [32] M.-H. Yu, H. Tsunoda, and M. Tsunoda, *Environmental toxicology: biological and health effects of pollutants*. crc press, 2005.
- [33] J. O. Nriagu, "A global assessment of natural sources of atmospheric trace metals," *Nature*, vol. 338, pp. 47–49, 1989.
- [34] W. Salomons, U. Förstner, and P. Mader, *Heavy metals: problems and solutions*. Springer Science & Business Media, 2012.
- [35] B. Volesky, "Removal and recovery of heavy metals," *Biosorption of heavy metals*, pp. 7–43, 1990.
- [36] N. Ahalya, T. Ramachandra, and R. Kanamadi, "Biosorption of heavy metals," *Res. J. Chem. Environ*, vol. 7, no. 4, pp. 71–79, 2003.
- [37] M. González and J. Silva, "Síntesis de nanopartículas de magnetita recubiertas de quitosano para la adsorción de cromo hexavalente." *Perfiles*, vol. 1, no. 29, pp. 78–89, 2023.

- [38] K. Shekhawat, S. Chatterjee, B. Joshi *et al.*, “Chromium toxicity and its health hazards,” *International Journal of Advanced Research*, vol. 3, no. 7, pp. 167–172, 2015.
- [39] A. Dayan and A. Paine, “Mechanisms of chromium toxicity, carcinogenicity and allergenicity: review of the literature from 1985 to 2000,” *Human & experimental toxicology*, vol. 20, no. 9, pp. 439–451, 2001.
- [40] T. Pavesi and J. C. Moreira, “Mechanisms and individuality in chromium toxicity in humans,” *Journal of applied toxicology*, vol. 40, no. 9, pp. 1183–1197, 2020.
- [41] R. M. Donaldson and R. F. Barreras, “Intestinal absorption of trace quantities of chromium,” *The Journal of laboratory and clinical medicine*, vol. 68, no. 3, pp. 484–493, 1966.
- [42] A. L. Rowbotham, L. S. Levy, and L. K. Shuker, “Chromium in the environment: an evaluation of exposure of the uk general population and possible adverse health effects,” *Journal of Toxicology and Environmental Health Part B: Critical Reviews*, vol. 3, no. 3, pp. 145–178, 2000.
- [43] A. Aitio, “Biological monitoring,” *Biological monitoring of toxic metals*, pp. 75–83, 1988.
- [44] G. Castillo-López, P. Salas-Cisneros, M. Logroño-Veloz, and M. Vinueza-Veloz, “Hexavalent chromium in waters for human consumption and irrigation in the guano canton,” *ESPOCH Congresses: The Ecuadorian Journal of STEAM*, pp. 524–532, 2021.
- [45] E. Matteoda, M. Blarasin, G. Damilano, A. Cabrera, and J. G. Albo, “Cromo en aguas subterráneas y superficiales en el entorno de una curtiembre, relación con valores de fondo natural. elena, córdoba. argentina,” *Revista del Instituto Geológico Minero de España (IGME)*, vol. 120, no. 4, pp. 617–630, 2009.
- [46] S. Peñarrieta Bravo, “Análisis de la política ambiental implementada por la ilustre municipalidad del cantón portoviejo en el período 2000-2004,” 2014.

- [47] M. A. Aegerter, N. Leventis, and M. M. Koebel, *Aerogels handbook*. Springer Science & Business Media, 2011.
- [48] E. J. S. Christy, A. Rajeswari, S. Gopi, and A. Pius, “Chitin and chitosan-based aerogels,” in *Handbook of Chitin and Chitosan*. Elsevier, 2020, pp. 285–334.
- [49] S. S. Kistler, “Coherent expanded aerogels and jellies,” *Nature*, vol. 127, no. 3211, pp. 741–741, 1931.
- [50] J. Fricke, “Aerogels and their applications,” *Journal of non-crystalline solids*, vol. 147, pp. 356–362, 1992.
- [51] M. Hasanpour and M. Hatami, “Application of three dimensional porous aerogels as adsorbent for removal of heavy metal ions from water/wastewater: A review study,” *Advances in Colloid and Interface Science*, vol. 284, 2020, cited By 135. [Online]. Available: <https://www.scopus.com/inward/record.uri?eid=2-s2.0-85090357096&doi=10.1016%2fj.cis.2020.102247&partnerID=40&md5=f05fef713b1f242f75a81b02152e9275>
- [52] I. Smirnova and P. Gurikov, “Aerogel production: Current status, research directions, and future opportunities,” *The Journal of Supercritical Fluids*, vol. 134, pp. 228–233, 2018.
- [53] X. Yang and E. D. Cranston, “Chemically cross-linked cellulose nanocrystal aerogels with shape recovery and superabsorbent properties,” *Chemistry of Materials*, vol. 26, no. 20, pp. 6016–6025, 2014.
- [54] H. Hosseini and S. M. Mousavi, “Bacterial cellulose/polyaniline nanocomposite aerogels as novel bioadsorbents for removal of hexavalent chromium: Experimental and simulation study,” *Journal of Cleaner Production*, vol. 278, p. 123817, 2021.
- [55] G. Crini, “Recent developments in polysaccharide-based materials used as adsorbents in wastewater treatment,” *Progress in polymer science*, vol. 30, no. 1, pp. 38–70, 2005.

- [56] H. Maleki, L. Durães, C. A. García-González, P. Del Gaudio, A. Portugal, and M. Mahmoudi, “Synthesis and biomedical applications of aerogels: Possibilities and challenges,” *Advances in colloid and interface science*, vol. 236, pp. 1–27, 2016.
- [57] Y. Tsutsumi, H. Koga, Z.-D. Qi, T. Saito, and A. Isogai, “Nanofibrillar chitin aerogels as renewable base catalysts,” *Biomacromolecules*, vol. 15, no. 11, pp. 4314–4319, 2014.
- [58] M. Yadav, P. Goswami, K. Paritosh, M. Kumar, N. Pareek, and V. Vivekanand, “Seafood waste: a source for preparation of commercially employable chitin/chitosan materials,” *Bioresources and Bioprocessing*, vol. 6, no. 1, pp. 1–20, 2019.
- [59] W. Amass, A. Amass, and B. Tighe, “A review of biodegradable polymers: uses, current developments in the synthesis and characterization of biodegradable polyesters, blends of biodegradable polymers and recent advances in biodegradation studies,” *Polymer international*, vol. 47, no. 2, pp. 89–144, 1998.
- [60] M. N. R. Kumar, “A review of chitin and chitosan applications,” *Reactive and functional polymers*, vol. 46, no. 1, pp. 1–27, 2000.
- [61] M. Rhazi, J. Desbrieres, A. Tolaimate, M. Rinaudo, P. Vottero, A. Alagui, and M. El Meray, “Influence of the nature of the metal ions on the complexation with chitosan.: Application to the treatment of liquid waste,” *European Polymer Journal*, vol. 38, no. 8, pp. 1523–1530, 2002.
- [62] M.-W. Wan, C.-C. Kan, B. D. Rogel, and M. L. P. Dalida, “Adsorption of copper (ii) and lead (ii) ions from aqueous solution on chitosan-coated sand,” *Carbohydrate Polymers*, vol. 80, no. 3, pp. 891–899, 2010.
- [63] H. Mansur, “de s. costa, e. jr., mansur, aap & barbosa-stancioli, ef cytocompatibility evaluation in cell-culture systems of chemically crosslinked chitosan/pva hydrogels,” *Mater. Sci. Eng. C*, vol. 29, pp. 1574–1583, 2009.
- [64] A. Ghosh and M. A. Ali, “Studies on physicochemical characteristics of chitosan derivatives with dicarboxylic acids,” *Journal of Materials Science*, vol. 47, pp. 1196–1204, 2012.

- [65] F.-L. Mi, H.-W. Sung, S.-S. Shyu, C.-C. Su, and C.-K. Peng, "Synthesis and characterization of biodegradable tpp/genipin co-crosslinked chitosan gel beads," *Polymer*, vol. 44, no. 21, pp. 6521–6530, 2003.
- [66] J. Khouri, A. Penlidis, and C. Moresoli, "Viscoelastic properties of crosslinked chitosan films," *Processes*, vol. 7, no. 3, p. 157, 2019.
- [67] P. Guerrero, A. Muxika, I. Zarandona, and K. De La Caba, "Crosslinking of chitosan films processed by compression molding," *Carbohydrate polymers*, vol. 206, pp. 820–826, 2019.
- [68] J. Varshousaz and R. Alinagari, "Effect of citric acid as cross-linking agent on insulin loaded chitosan microspheres," 2005.
- [69] D. M. Ruthven, *Principles of adsorption and adsorption processes*. John Wiley & Sons, 1984.
- [70] H. Mittal, A. Maity, and S. Sinha Ray, "The adsorption of pb²⁺ and cu²⁺ onto gum ghatti-grafted poly (acrylamide-co-acrylonitrile) biodegradable hydrogel: isotherms and kinetic models," *The Journal of Physical Chemistry B*, vol. 119, no. 5, pp. 2026–2039, 2015.
- [71] T. R. Sahoo and B. Prelot, "Adsorption processes for the removal of contaminants from wastewater: the perspective role of nanomaterials and nanotechnology," in *Nanomaterials for the detection and removal of wastewater pollutants*. Elsevier, 2020, pp. 161–222.
- [72] N. Ayawei, A. N. Ebelegi, and D. Wankasi, "Modelling and interpretation of adsorption isotherms," *Journal of chemistry*, vol. 2017, 2017.
- [73] S. D. Faust and O. M. Aly, *Adsorption processes for water treatment*. Elsevier, 2013.
- [74] X. Chen, "Modeling of experimental adsorption isotherm data," *information*, vol. 6, no. 1, pp. 14–22, 2015.

- [75] A. Günay, E. Arslankaya, and I. Tosun, "Lead removal from aqueous solution by natural and pretreated clinoptilolite: adsorption equilibrium and kinetics," *Journal of hazardous materials*, vol. 146, no. 1-2, pp. 362–371, 2007.
- [76] A. Proctor and J. Toro-Vazquez, "The freundlich isotherm in studying adsorption in oil processing," *Journal of the American Oil Chemists' Society*, vol. 73, pp. 1627–1633, 1996.
- [77] N. Ayawei, A. T. Ekubo, D. Wankasi, and E. D. Dikio, "Adsorption of congo red by ni/al-co₃: equilibrium, thermodynamic and kinetic studies," *Oriental Journal of Chemistry*, vol. 31, no. 3, p. 1307, 2015.
- [78] F. Brouers and T. J. Al-Musawi, "On the optimal use of isotherm models for the characterization of biosorption of lead onto algae," *Journal of Molecular Liquids*, vol. 212, pp. 46–51, 2015.
- [79] A. Kiselev, "Vapor adsorption in the formation of adsorbate molecule complexes on the surface," *Kolloid Zhur*, vol. 20, pp. 338–348, 1958.
- [80] U. Upadhyay, I. Sreedhar, S. A. Singh, C. M. Patel, and K. Anitha, "Recent advances in heavy metal removal by chitosan based adsorbents," *Carbohydrate Polymers*, vol. 251, p. 117000, 2021.
- [81] S. Raghav and D. Kumar, "Adsorption equilibrium, kinetics, and thermodynamic studies of fluoride adsorbed by tetrametallic oxide adsorbent," *Journal of Chemical & Engineering Data*, vol. 63, no. 5, pp. 1682–1697, 2018.
- [82] J. Febrianto, A. N. Kosasih, J. Sunarso, Y.-H. Ju, N. Indraswati, and S. Ismadji, "Equilibrium and kinetic studies in adsorption of heavy metals using biosorbent: a summary of recent studies," *Journal of hazardous materials*, vol. 162, no. 2-3, pp. 616–645, 2009.
- [83] S. Lagergren, "Zur theorie der sogenannten adsorption gelöster stoffe," *Kungliga svenska vetenskapsakademiens. Handlingar*, vol. 24, pp. 1–39, 1898.

- [84] O. K. Alkadir, Z. I. Al-Mashhadani, A. M. Aljeboree, and A. F. Alkaim, "Comparison between pseudo-first-order and pseudo-second-order of linear and nonlinear equations adsorption kinetic models for the removal of amoxicillin (amx) onto hydrogel."
- [85] G. W. Kajjumba, S. Emik, A. Öngen, H. K. Özcan, and S. Aydın, "Modelling of adsorption kinetic processes—errors, theory and application," *Advanced sorption process applications*, pp. 1–19, 2018.
- [86] Y.-S. Ho and G. McKay, "Pseudo-second order model for sorption processes," *Process biochemistry*, vol. 34, no. 5, pp. 451–465, 1999.
- [87] A. K. Cordova Estrada, F. Cordova Lozano, and R. A. Lara Díaz, "Thermodynamics and kinetic studies for the adsorption process of methyl orange by magnetic activated carbons," *Air, Soil and Water Research*, vol. 14, p. 11786221211013336, 2021.
- [88] A. Darwish, M. Rashad, and H. A. AL-Aoh, "Methyl orange adsorption comparison on nanoparticles: Isotherm, kinetics, and thermodynamic studies," *Dyes and Pigments*, vol. 160, pp. 563–571, 2019.
- [89] T. Zuyi and C. Taiwei, "On the applicability of the langmuir equation to estimation of adsorption equilibrium constants on a powdered solid from aqueous solution," *Journal of colloid and interface science*, vol. 231, no. 1, pp. 8–12, 2000.
- [90] K.-H. Houg and D.-Y. Lee, "Comparisons of linear and nonlinear langmuir and freundlich curve-fit in the study of cu, cd and pb adsorption on taiwan soils," *Soil Science*, vol. 163, no. 2, pp. 115–121, 1998.
- [91] X. Zhou, H. Liu, and J. Hao, "Letters to the editor," *Adsorption Science & Technology*, vol. 30, no. 7, pp. 647–649, 2012. [Online]. Available: <https://doi.org/10.1260/0263-6174.30.7.647>
- [92] P. G. Ponnusamy, J. Sundaram, and S. Mani, "Preparation and characterization of citric acid crosslinked chitosan-cellulose nanofibrils composite films for packaging applications," *Journal of Applied Polymer Science*, vol. 139, no. 17, p. 52017, 2022.

- [93] N. Saadatkhan, A. Carillo Garcia, S. Ackermann, P. Leclerc, M. Latifi, S. Samih, G. S. Patience, and J. Chaouki, “Experimental methods in chemical engineering: Thermogravimetric analysis—tga,” *The Canadian Journal of Chemical Engineering*, vol. 98, no. 1, pp. 34–43, 2020.
- [94] G. Alberti and G. Nuzzaci, “1.6. 5 sem and tem techniques,” in *World Crop Pests*. Elsevier, 1996, vol. 6, pp. 399–410.
- [95] W. Mäntele and E. Deniz, “Uv–vis absorption spectroscopy: Lambert-beer reloaded,” pp. 965–968, 2017.
- [96] J. H. R. Llanos, L. C. de Oliveira Vercik, A. Vercik *et al.*, “Physical properties of chitosan films obtained after neutralization of polycation by slow drip method,” *Journal of Biomaterials and Nanobiotechnology*, vol. 6, no. 04, p. 276, 2015.
- [97] M. F. Bósquez-Cáceres, L. D. Lima, V. Morera Córdova, A. D. Delgado, J. Béjar, N. Arjona, L. Álvarez-Contreras, and J. P. Tafur, “Chitosan-carboxymethylcellulose hydrogels as electrolytes for zinc–air batteries: An approach to the transition towards renewable energy storage devices,” *Batteries*, vol. 8, no. 12, p. 265, 2022.
- [98] A. A. Moosa, A. M. Ridha, and N. A. Kadhim, “Use of biocomposite adsorbents for the removal of methylene blue dye from aqueous solution,” *American Journal of Materials Science*, vol. 6, no. 5, pp. 135–146, 2016.
- [99] X. Ma, W. Zhong, J. Zhao, S. L. Suib, and Y. Lei, ““self-heating” enabled one-pot synthesis of fluorescent carbon dots,” *Engineered Science*, vol. 9, 2019.
- [100] E. Szymañska and K. Winnicka, “Stability of chitosan—a challenge for pharmaceutical and biomedical applications,” *Marine drugs*, vol. 13, no. 4, pp. 1819–1846, 2015.
- [101] M. M. Barbooti and D. A. Al-Sammerrai, “Thermal decomposition of citric acid,” *Thermochimica acta*, vol. 98, pp. 119–126, 1986.
- [102] A. Bahiraei and J. Behin, “Effect of citric acid and sodium chloride on characteristics of sunflower seed shell-derived activated carbon,” *Chemical Engineering & Technology*, vol. 44, no. 9, pp. 1604–1617, 2021.

- [103] D. R. Rohindra, A. V. Nand, and J. R. Khurma, "Swelling properties of chitosan hydrogels," *The South Pacific Journal of Natural and Applied Sciences*, vol. 22, no. 1, pp. 32–35, 2004.
- [104] W. Zhu, X. Jiang, F. Liu, F. You, and C. Yao, "Preparation of chitosan—graphene oxide composite aerogel by hydrothermal method and its adsorption property of methyl orange," *Polymers*, vol. 12, no. 9, p. 2169, 2020.
- [105] T. S. Badessa, E. Wakuma, and A. M. Yimer, "Bio-sorption for effective removal of chromium (vi) from wastewater using moringa stenopetala seed powder (mssp) and banana peel powder (bpp)," *BMC chemistry*, vol. 14, pp. 1–12, 2020.
- [106] T. Kekes, G. Kolliopoulos, and C. Tzia, "Hexavalent chromium adsorption onto crosslinked chitosan and chitosan/ β -cyclodextrin beads: Novel materials for water decontamination," *Journal of Environmental Chemical Engineering*, vol. 9, no. 4, p. 105581, 2021.
- [107] V. N. Tirtom, A. Dincer, S. Becerik, T. Aydemir, and A. Çelik, "Removal of lead (ii) ions from aqueous solution by using crosslinked chitosan-clay beads," *Desalination and water treatment*, vol. 39, no. 1-3, pp. 76–82, 2012.
- [108] J. Thilagan, S. Gopalakrishnan, and T. Kannadasan, "A study on adsorption of copper (ii) ions in aqueous solution by chitosan-cellulose beads cross linked by formaldehyde," *International journal of pharmaceutical and chemical sciences*, vol. 2, no. 2, pp. 1043–1054, 2013.
- [109] S. J. Tshemese, W. Mhike, and S. M. Tichapondwa, "Adsorption of phenol and chromium (vi) from aqueous solution using exfoliated graphite: equilibrium, kinetics and thermodynamic studies," *Arabian Journal of Chemistry*, vol. 14, no. 6, p. 103160, 2021.
- [110] N. Kumara, N. Hamdan, M. I. Petra, K. U. Tennakoon, and P. Ekanayake, "Equilibrium isotherm studies of adsorption of pigments extracted from kuduk-kuduk (*Melastoma malabathricum* l.) pulp onto tio₂ nanoparticles," *Journal of Chemistry*, vol. 2014, 2014.

- [111] S. Lyubchik, A. Lyubchik, O. Lygina, S. Lyubchik, and I. Fonseca, “Comparison of the thermodynamic parameters estimation for the adsorption process of the metals from liquid phase on activated carbons,” in *Thermodynamics-Interaction Studies-Solids, Liquids and Gases*. IntechOpen, 2011.
- [112] J. V. Salinas Vásquez, “El cuero, producción industrial y artesanal en el ecuador análisis comparativo sobre el método de producción del cuero entre las provincias de tungurahua y azuay,” B.S. thesis, Universidad del Azuay, 2014.
- [113] M. J. Silva and D. Salinas Morales, “La contaminación proveniente de la industria curtiembre, una aproximación a la realidad ecuatoriana,” *Revista Científica UIS-RAEL*, vol. 9, no. 1, pp. 69–80, 2022.
- [114] A. Riofrio, T. Alcivar, and H. Baykara, “Environmental and economic viability of chitosan production in guayas-ecuador: a robust investment and life cycle analysis,” *ACS omega*, vol. 6, no. 36, pp. 23 038–23 051, 2021.
- [115] Alibaba.com. [Online]. Available: <https://www.alibaba.com/>
- [116] H. E. Parra Gutiérrez *et al.*, “Diseño y construcción de un liofilizador para el secado de plantas aromáticas,” 2015.